



## Original article

# Structural modifications of 4-aryl-4-oxo-2-aminybutanamides and their acetyl- and butyrylcholinesterase inhibitory activity. Investigation of AChE–ligand interactions by docking calculations and molecular dynamics simulations



Maja D. Vitorović-Todorović<sup>a,\*</sup>, Catherine Koukoulitsa<sup>b</sup>, Ivan O. Juranić<sup>c</sup>,  
Ljuba M. Mandić<sup>d</sup>, Branko J. Drakulić<sup>c</sup>

<sup>a</sup> Military Technical Institute, Ratka Resanovića 1, Belgrade, Serbia

<sup>b</sup> Department of Chemistry, University of Athens, Panepistimiopolis-Zografou, 15771, Greece

<sup>c</sup> Department of Chemistry-ICHM, University of Belgrade, Njegoševa 12, Belgrade, Serbia

<sup>d</sup> Faculty of Chemistry, University of Belgrade, Studentski trg 12-16, Belgrade, Serbia

## ARTICLE INFO

## Article history:

Received 26 December 2013

Received in revised form

31 March 2014

Accepted 1 May 2014

Available online 4 May 2014

## Keywords:

4-Aryl-4-oxo-2-aminybutanamides

Anticholinesterase activity

Mixed type reversible inhibitors

Docking study

Molecular dynamics

## ABSTRACT

Congeneric set of thirty-eight 4-aryl-4-oxo-2-(*N*-aryl/cycloalkyl)butanamides has been designed, synthesized and evaluated for acetyl- and butyrylcholinesterase inhibitory activity. Structural variations included cycloalkylamino group attached to C2 position of butanoyl moiety, and variation of amido moiety of molecules. Twelve compounds, mostly piperidino and imidazolo derivatives, inhibited AChE in low micromolar range, and were inactive toward BChE. Several *N*-methylpiperazino derivatives showed inhibition of BChE in low micromolar or submicromolar concentrations, and were inactive toward AChE. Therefore, the nature of the cycloalkylamino moiety governs the AChE/BChE selectivity profile of compounds. The most active AChE inhibitor showed mixed-type inhibition modality, indicating its binding to free enzyme and to enzyme–substrate complex. Thorough docking calculations of the seven most potent AChE inhibitors from the set, showed that the hydrogen bond can be formed between amide –NH– moiety of compounds and –OH group of Tyr 124. The 10 ns unconstrained molecular dynamic simulation of the AChE–compound **18** complex shows that this interaction is the most persistent. This is, probably, the major anchoring point for the binding.

© 2014 Elsevier Masson SAS. All rights reserved.

## 1. Introduction

Acetylcholinesterase (AChE) is a carboxylesterase which terminates cholinergic neuro-transmission, by hydrolyzing neurotransmitter acetylcholine (ACh) in a synaptic cleft. Reversible AChE inhibition is implicated in a number of disorders, including Alzheimer's disease (AD) [1], Myasthenia gravis [2], glaucoma [3], and can be used as a pretreatment against nerve agents' intoxications [4,5]. Recently, AChE's sister enzyme butyrylcholinesterase, also became important as pharmacological target for AD. BChE is capable to compensate AChE catalytic functions in synaptic cleft

[6,7] and its activity significantly rises during time course in AD [8,9]. Therefore, in designing and testing of reversible inhibitors it is advisable to monitor activity toward both enzymes.

AChE contains 20 Å deep and narrow gorge, in which five regions that are involved in the substrate, irreversible and reversible inhibitor binding, can be distinguished (human and *electric eel* AChE numbering): (1) catalytic triad residues: Ser 203, His 447, and Glu 334 [10], at the bottom of the gorge, which directly participate in catalytic cycle, by charge relay mechanism, as in other serine esterases; (2) oxyanion hole: is an arrangement of hydrogen bond donors which stabilize the transient tetrahedral enzyme–substrate complex by accommodation of negatively charged carbonyl oxygen. This region inside the active center is formed by backbone –NH– groups of amino acid residues Gly 121, Gly 122 and Ala 204 [11,12]; (3) the 'anionic site' (AS), where Trp 86 is situated. This residue is conserved in all cholinesterases and

\* Corresponding author.

E-mail addresses: [mvitod@chem.bg.ac.rs](mailto:mvitod@chem.bg.ac.rs), [majavitod@gmail.com](mailto:majavitod@gmail.com) (M.D. Vitorović-Todorović).

it is involved in orientation and stabilization of trimethylammonium group of AChE, by forming cation- $\pi$  interactions [13–16]; (4) acyl pocket comprises two phenylalanine residues, 295 and 297, which interact with the substrate acyl group. They form the clamps around methyl group, and decrease its degrees of freedom [17]; (5) peripheral anionic site (PAS) [18–20], comprises residues which are located at the rim of the active site gorge, Tyr 72, Tyr 124, Trp 286 and Asp 74. Possible binding sites for the reversible inhibitors comprise both AS and PAS. The so-called dimeric (dual) inhibitors bind simultaneously to both of these sites. In BChE active site, six out of fourteen aromatic amino acid residues in AChE (Tyr 72, Tyr 124, Trp 286, Phe 295, Phe 297 and Tyr 337) are replaced by aliphatic ones (Asn 68, Gln 119, Ala 277, Leu 286, Val 288, and Ala 328). This causes 200 Å<sup>3</sup> larger active site gorge of BChE, comparing to that of AChE. Therefore, BChE is capable to hydrolyze wide variety of esters [21].

Recently, we reported congeneric series of the twenty 4-aryl-4-oxo-2-aminybutanamides, with variation of substituents on the aroyl phenyl ring, while phenylamido moiety was retained unchanged [22]. Alkyl substituted congeners inhibited both AChE and BChE in micromolar concentrations, while chloro- or methoxy-substituted compounds were proved as inactive. The nature of cycloalkylamino moiety of molecules governed the AChE/BChE selectivity: piperidino and imidazolo derivatives were active toward AChE, while morpholino derivatives were active toward BChE.

In the present work, we investigated the influence of the amido moiety variation on AChE and BChE inhibition potency and selectivity. We systematically changed the cyclic amine used to obtain precursor aroylacrylic acid amides (3,5-dimethoxyaniline, 4-isopropylaniline and cyclohexylaniline), retaining the favorable alkyl substituents (4-*i*-Pr, 2,4-di-*i*-Pr and  $\beta$ -tetralinyl) on the aroyl part of the molecule. For the Michael addition on the activated double bond, four amines were used: piperidine, imidazole, morpholine and *N*-methylpiperazine. Along with this, two more compounds were synthesized. To test the effects of the presence of highly voluminous moiety at position C2 of the butanoic scaffold on the AChE and BChE inhibition activity, we synthesized addition products of 4-benzylpiperidine on the 4-(4-*i*-Pr-Ph)-4-oxo-2-butenic acid phenylamide, and of 4-(2-*N,N*-di-Me-aminoethyl)-1-piperazine on the 4-(4-*i*-Pr-Ph)-4-oxo-2-butenic acid 3,5-di-MeO-phenylamide. The last derivative comprises moiety that mimick trimethylaminoethyl group of the acetylcholine. Overall, thirty-eight compounds were prepared and their AChE and BChE inhibition activity determined. Possible interactions of the most potent derivatives with the AChE active site residues were further investigated by docking calculations and by molecular dynamics.

## 2. Results and discussion

### 2.1. Chemistry

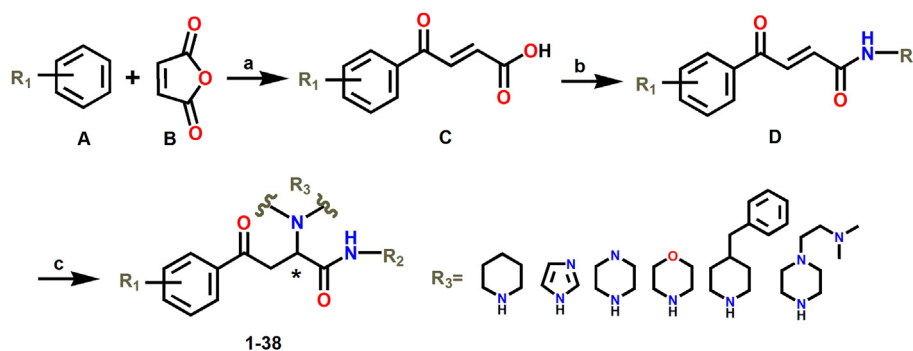
Synthetic path to **1–38** is given in Scheme 1. Friedel–Crafts acylation of the commercially available substituted benzenes (**A**) with maleic acid anhydride (**B**) yields aroylacrylic acids (**C**) [23]. Subsequently, acids were converted to acid chlorides in dry THF by phosphorous-oxychloride, then *in situ* reacted with equimolar amounts of primary amine (3,5-dimethoxyaniline, 4-isopropylaniline and cyclohexylaniline) to give the corresponding amides (**D**) [24]. Michael addition of the cyclic amines (piperidine, imidazole, morpholine, *N*-methylpiperazine, 4-benzylpiperidine and 4-(2-*N,N*-di-Me-aminoethyl)-1-piperazine) proceeded smoothly to give target compounds **1–38**.

### 2.2. Structure–activity relationships

Inhibition potency of the compounds **1–38** toward AChE and BChE, given as IC<sub>50</sub> values, are shown in Table 1, along with potency data of the previously published congeners having unsubstituted phenylamido moiety (**1a–9a**) [22]. Due to limited solubility of some derivatives, we were unable to obtain entire dose–response curve (spanning range of 20–80% of the enzyme activity inhibition). For those compounds we reported the percent of the residual enzyme activity at the highest concentration tested.

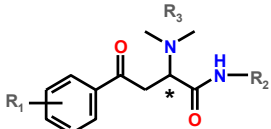
Twelve compounds, out of twenty that inhibited AChE activity, were active in low micromolar concentrations. Most of the piperidino and imidazolo derivatives showed inhibition of AChE in low micromolar range, while morpholino and *N*-methylpiperazino derivatives were inactive up to concentrations of 15–20  $\mu$ M. Clearly, the presence of bulkier substituents in position C2 of the butanoyl moiety of molecules reduces anti-AChE activity. Similar trend was also observed with previously synthesized compounds [22].

3,5-Dimethoxy substitution at phenylamido moiety of the imidazolo and piperidino derivatives, in some instances (compare **2** with **2a**, and **26** with **8a**) only slightly enhanced inhibition potency, while in others (compare **13** with **4a**, **14** with **5a** and **25** with **7a**) only slightly diminished inhibition potency. 4-Isopropyl substituted phenylamido moiety in piperidino and imidazolo derivatives, in most cases (**6**, **17**, **18**, **30**) slightly improved anti-AChE inhibition potency, comparing to the unsubstituted counterparts (**2a**, **4a**, **5a** and **8a**). In some instances, 4-*i*-Pr substitution had clearly beneficial influence on anti-AChE activity. This is especially evident in compounds **19** and **20**, in which this type of substitution turns inactive morpholino and *N*-methylpiperazino derivatives into active ones, with IC<sub>50</sub> values around 6.5  $\mu$ M.



**Scheme 1.** Synthetic path to **1–38**. Reagents: (a) AlCl<sub>3</sub>/CH<sub>2</sub>Cl<sub>2</sub>; (b) POCl<sub>3</sub>, dry THF. R<sub>2</sub> = 3,5-dimethoxyaniline, 4-isopropylaniline, or cyclohexylaniline; (c) toluene, CH<sub>2</sub>Cl<sub>2</sub> and R<sub>3</sub> = piperidine, imidazole, morpholine, *N*-methylpiperazine, 4-benzylpiperidine and 4-(2-*N,N*-di-Me-aminoethyl)-1-piperazine.

**Table 1**  
An *in vitro* AChE and BChE inhibition assay data for compounds **1–38** and **1a–9a**.

				IC <sub>50</sub> ± SEM (μM) <sup>a</sup>	
Comp. no.	R <sub>1</sub>	R <sub>2</sub>	R <sub>3</sub>	AChE	BChE
<b>1</b>	4- <i>i</i> -Pr	3,5-di-OMe-Ph-	Piperidine	Unstable <sup>b</sup>	Unstable
<b>2</b>			Imidazole	4.49 ± 0.18	>20
<b>3</b>			Morpholine	>20	>20
<b>4</b>			<i>N</i> -Me-piperazine	76.65 @ 20 <sup>c</sup>	>20
<b>5</b>		4- <i>i</i> -Pr-Ph-	Piperidine	Unstable	Unstable
<b>6</b>			Imidazole	2.33 ± 0.40	>20
<b>7</b>			Morpholine	>20	>20
<b>8</b>			<i>N</i> -Me-piperazine	>20	72.41 @ 15
<b>9</b>		Ch-	Piperidine	63.10 @ 15	64.96 @ 20
<b>10</b>			Imidazole	65.31 @ 15	76.01 @ 20
<b>11</b>			Morpholine	85.13 @ 25	46.82 @ 10
<b>12</b>			<i>N</i> -CH <sub>3</sub> piperazine	86.24 @ 25	66.18 @ 20
<b>13</b>	2,4-di- <i>i</i> -Pr	3,5-di-OMe-Ph-	Piperidine	>7.5	>7.5
<b>14</b>			Imidazole	3.30 ± 0.35	78.37 @ 20
<b>15</b>			Morpholine	>20	62.37 @ 10
<b>16</b>			<i>N</i> -Me-piperazine	>20	5.26 ± 0.24
<b>17</b>		4- <i>i</i> -Pr-Ph-	Piperidine	1.96 ± 0.22	Insoluble
<b>18</b>			Imidazole	2.05 ± 0.06	>20
<b>19</b>			Morpholine	44.36 @ 6.5	73.56 @ 10
<b>20</b>			<i>N</i> -Me-piperazine	43.64 @ 6.5	0.74 ± 0.16
<b>21</b>		Ch-	Piperidine	5.44 ± 0.61	72.73 @ 20
<b>22</b>			Imidazole	5.94 ± 0.02	65.83 @ 20
<b>23</b>			Morpholine	>15	>20
<b>24</b>			<i>N</i> -Me-piperazine	>15	2.25 ± 0.23
<b>25</b>	β-Tetralinyl	3,5-di-OMe-Ph-	Piperidine	6.37 ± 1.02	>20
<b>26</b>			Imidazole	3.23 ± 0.15	>20
<b>27</b>			Morpholine	Insoluble	Insoluble
<b>28</b>			<i>N</i> -Me-piperazine	>15	56.68 @ 20
<b>29</b>		4- <i>i</i> -Pr-Ph-	Piperidine	Insoluble	Insoluble
<b>30</b>			Imidazole	2.36 ± 0.20	>20
<b>31</b>			Morpholine	>15	>15
<b>32</b>			<i>N</i> -Me-piperazine	86.48 @ 8.5	10.75 ± 1.39
<b>33</b>		Ch-	Piperidine	>20	61.46 @ 20
<b>34</b>			Imidazole	19.99 ± 2.00	52.23 @ 20
<b>35</b>			Morpholine	>15	75.22 @ 20
<b>36</b>			<i>N</i> -Me-piperazine	>20	39.10 @ 20
<b>37</b>	4- <i>i</i> -Pr	-Ph	4-Benzylpiperidine	>20	>20
<b>38</b>	4- <i>i</i> -Pr	3,5-di-OMe-Ph-	4-(2- <i>N,N</i> -di-Me-aminoethyl)-1-piperazine	>20	>20
<b>1a</b>	4- <i>i</i> -Pr	-Ph	Piperidine	3.47 ± 0.04	7.06 ± 0.04
<b>2a</b>			Imidazole	8.22 ± 0.04	90.00 @ 30
<b>3a</b>			Morpholine	>100	72.78 @ 40
<b>4a</b>	2,4-di- <i>i</i> -Pr	-Ph	Piperidine	4.86 ± 0.03	60.07 @ 15
<b>5a</b>			Imidazole	1.55 ± 0.01	>20
<b>6a</b>			Morpholine	>10	2.48 ± 0.01
<b>7a</b>	β-Tetralinyl	-Ph	Piperidine	5.64 ± 0.02	78.50 @ 15
<b>8a</b>			Imidazole	6.34 ± 0.01	83.00 @ 40
<b>9a</b>			Morpholine	>30	87.00 @ 40
<b>Tacrine</b>	/	/	/	42.95 ± 0.01 nM	6.95 ± 0.01 nM

<sup>a</sup> Concentration required to produce 50% inhibition of AChE (*electric eel*) or BChE (equine serum). IC<sub>50</sub> values are given as the mean of three independent determinations.

<sup>b</sup> Decomposition of the compounds in the enzyme inhibition assay was observed.

<sup>c</sup> Inhibition potency of the compounds was expressed as percent of residual enzyme activity at the given concentration.

The change of the phenyl moiety to cyclohexyl on amido part of the piperidino and imidazolo derivatives (**9**, **10**, **33**, **34**) reduced anti-AChE activity for at least one order of magnitude. This indicates that amido moiety of the molecules probably interacts with AChE active site residues involving  $\pi$  electrons of the phenyl ring. The decrease in inhibition potency, due to the presence of cyclohexyl moiety, was modest only for 2,4-di-*i*-Pr-substituted piperidino and imidazolo derivatives **21** and **22**, with IC<sub>50</sub> values of 5.44 and 5.94 μM, respectively.

Nineteen derivatives influenced BChE activity (expressed as residual enzyme activity at highest concentration tested, Table 1),

but only three compounds had IC<sub>50</sub> values in low micromolar (**16** and **24**), or submicromolar concentrations (**20**). All three compounds bear 2,4-di-*i*-Pr-substituted aroyl and *N*-methylpiperazino moieties. We expected that, due to a larger BChE active site gorge, bulkier substituents on phenylamido moiety will increase potency of compounds comparing to unsubstituted derivatives, described earlier. Surprisingly, 2,4-di-*i*-Pr morpholino derivatives (**15** and **19**) with 3,5-dimethoxy or 4-isopropyl substituents on phenylamido moiety did not appear more potent, comparing to unsubstituted derivative **6a** reported in previous work (IC<sub>50</sub> = 2.48 μM). β-Tetralinyl substituted *N*-methylpiperazino derivatives **28**, **32** and **36**,

appeared moderately potent, with  $IC_{50}$  values in the range of 10–20  $\mu$ M. All other compounds didn't produce significant inhibition of BChE activity.

To test the effects of the presence of highly voluminous moiety at position C2 of the butanoic moiety of molecules on the AChE and BChE inhibition activity, we synthesized derivative **37**, by the addition of 4-benzylpiperidine. We aimed to test whether this group will cause an increase in inhibition potency and whether such compound has different mode of binding to enzyme active site (to PAS instead to AS), comparing to other derivatives. In compound **38**, we introduced dimethylaminoethyl moiety, a group that mimick trimethylaminoethyl group of ACh. Unfortunately, both derivatives appeared inactive at the highest concentration tested (20  $\mu$ M).

The spectrophotometric method of Ellman was used to determine the type of inhibition and the  $K_i$  for derivative **17**, most active toward AChE. Compound exhibited mixed type of inhibition. This behavior was indicated by intersection of double reciprocal lines in the upper left quadrant of Lineweaver–Burk plot, shown in Fig. 1 and Table S1, Supplementary information. Generally, this type of inhibition indicates binding to free enzyme and enzyme–substrate complex; that is, a possible binding to the site distant from the active site. The  $K_i$ 's obtained were 0.52  $\mu$ M (binding to free enzyme) and 1.93  $\mu$ M (binding to enzyme–substrate complex).

### 2.3. Molecular modeling

3D-QSAR model described in previous article [22] was used to predict potency of compounds for which we obtained  $IC_{50}$  values in this study. Fair predictivity was obtained for compounds **2**, **6**, **14**, **17**, **18**, **21**, **22**, **25**, **26** and **30** ( $r^2 = 0.60$ ,  $sd = 0.118$ ); while potency of the compound **34** was overestimated in some extent. Results are given in Table S2 in Supplementary Material.

Along with this, we built independent 3D QSAR model by GRIND-2 descriptors for all compounds for which  $IC_{50}$  values toward AChE were obtained, reported in this, and in previous study [22]. In this model we also included compounds for which we obtained residual enzyme activity on defined concentration of the inhibitor (**4**, **9–12**, **19**, **20** and **32**). For the later subset of compounds we estimated  $IC_{50}$  values. For model building all available GRID probes were used, DRY (hydrophobic), N1 (HBD), O (HBA) and TIP

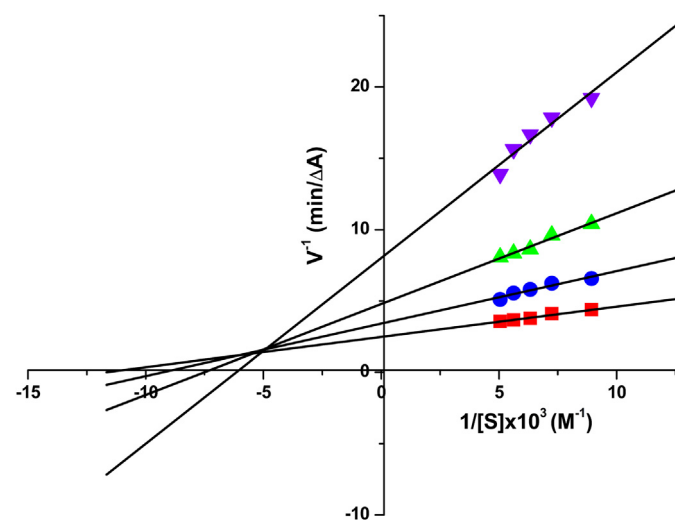


Fig. 1. Lineweaver–Burk plot of AChE (0.02 U) with substrate acetylthiocholine, in the absence and in presence of different concentrations of **17**. (■) No inhibitor; (●) 2  $\mu$ M; (▲) 4  $\mu$ M; (▼) 5  $\mu$ M.

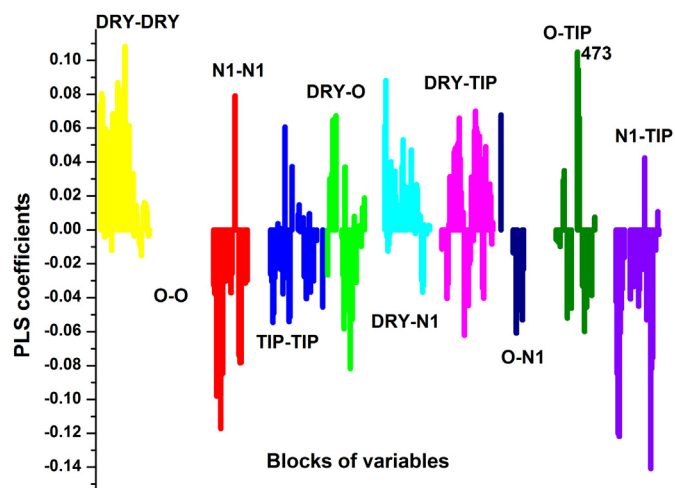


Fig. 2. PLS coefficients plot, obtained with 3LV.

(shape probe). PLS coefficients plot for the model obtained with 3LV are shown in Fig. 2. Although we didn't included shape probe in the model reported in previous work, because this model contained structurally diverse set of compounds, and good results were obtained using hydrophobic, HBD and HBA probes; DRY-DRY, N1-N1 and DRY-O blocks, common for both models, resemble each other. DRY-DRY block is filled with variables positively correlated with potency of compounds, implying positive contribution of hydrophobic moieties of compounds to activity. Although variables were expressed for all compounds in the set, higher intensity of variables for the most potent compounds in this block can be observed, comparing to least potent ones. This implies stronger hydrophobic interactions that most potent compounds can make with the respective biological target. Heatmaps of DRY-DRY block are depicted in Fig. S3a in Supplementary Material. It should be noted that we also observed rough positive trend between potency of compounds and their apolar surface areas calculated from 3D structures (data not shown). In N1-N1 block majority of variables are negatively correlated with potency of compounds. Heatmaps of N1-N1 block also show higher intensity of variables associated with less potent compounds, comparing to more potent ones, Fig. S3b in Supplementary Material. Variable O-TIP 473 (10.0–10.4 Å), has the highest positive impact on the overall model. It is expressed for the most active derivatives and connects MIF's of HBA probe (O), associated with amido –NH– group, and MIF's of shape (TIP) probe associated with substituents on the phenylamido ring (4-*i*-Pr or 3,5-di-OMe, Fig. S4 and Table S5, Supplementary Material). For compounds with unsubstituted phenylamido moiety TIP node is associated with substituents on aroyl phenyl ring. The 5LV PCA model explains about 55% variability in the set (Table S6, Supplementary Material). Statistics of the model is shown in Table 2. Reported  $r^2$  and  $q^2$  values were obtained after one cycle of the variable selection by fractional factorial design. Experimental and calculated  $p(IC_{50})$  values, obtained with 3 LV, are shown in Table S5 in Supplementary Material.

To explore possible ligand-AChE interactions, seven compounds with  $IC_{50}$  values below 5  $\mu$ M were docked into the AChE active site. Both enantiomers of the each compound were docked in mAChE (*Mus musculus*, PDB entry 2HA2), using the latest version of AutoDock 4 package [25]. Fifty binding poses were generated in each docking calculation. As the scoring functions used for prioritization of the obtained poses are still mostly inaccurate [26], we decided to analyze the most favorable binding pose (according to the estimated free energy of binding,  $\Delta G$ ) along with the best pose,



**Table 2**  
PLS model.

Component	SSX	SSX <sub>acc</sub>	SDEC	SDEP	R <sup>2</sup>	R <sup>2</sup> <sub>acc</sub>	Q <sup>2</sup> <sub>acc</sub>	LOO	Q <sup>2</sup> <sub>acc</sub>	LTO	Q <sup>2</sup> <sub>acc</sub>	RG
1	24.16	24.16	0.25	0.32	0.63	0.63	0.40		0.41		0.41	
2	14.99	39.16	0.14	0.23	0.25	0.88	0.68		0.67		0.65	
3	6.93	46.09	0.09	0.20	0.07	0.96	0.76		0.74		0.72	
4	11.46	57.55	0.07	0.20	0.02	0.97	0.76		0.75		0.73	
5	4.55	62.10	0.04	0.20	0.02	0.99	0.77		0.76		0.73	

Abbreviations: SSX, X variable explanation; SDEC, standard deviation of error of calculation; SDEP standard deviation of error of prediction; The 'acc' states for cumulative value; Validation methods used for calculation of  $q^2$  are: leave one out (LOO), leave two out (LTO) and random groups (RG). Four random groups were used.

belonging to the most populated cluster, by LigPlot program [27]. Detailed data with the list of all ligand-AChE interactions are given in Table 3. It should be noted that in both types of docking poses (best ranked pose and the most populated one), for all compounds shown in Table 3, the hydrogen bond between amide –NH– group of the compounds and –OH group of Tyr 124 side chain is formed. Also, in significant number of poses, a hydrogen bond between Phe 295 backbone –NH– group and different moieties of ligands (phenylamido –OCH<sub>3</sub> group, N3 nitrogen of imidazole ring, or aroyl carbonyl group) is formed. The residues which form hydrophobic interactions with docked compounds, in majority of poses, are His 447, Tyr 341, Phe 295, Phe 297 and Phe 338.

The overall description of the docking poses for all compounds is beyond the scope of this article. In the following lines we will provide detailed discussion of the obtained docking solutions for the three most potent derivatives, **6**, **17** and **18**, shown in Fig. 3. The *S* enantiomers are colored cyan and the *R* are colored red. Surprisingly, we found that *R* and *S* enantiomers of the each compound were docked in a mutually very similar fashion. The RMSD differences between atomic positions of docked poses of two enantiomers were less than 2.077 Å (heavy atom superposition), Table S7 in Supplementary Material. In Fig. 3a and b the docking solutions best ranked by the estimated free energy of binding ( $\Delta G$ ), for the compounds **17** and **18**, are shown. Both enantiomers of both compounds are oriented within the AChE active site gorge in the similar fashion. The aroyl moieties are oriented toward the bottom of the gorge, interacting with Trp 86 and Tyr 337 residues. Amido –NH– groups of the compounds form hydrogen bond with the side chain –OH group of Tyr 124. Phenylamido rings of both compounds are directed toward the entrance of the gorge (PAS) and interact with side chains of Trp 286, Phe 295 and Phe 297. The piperidine ring of compound **17** and the imidazole ring of compound **18** are found in the close proximity of catalytic triad residues, His 447 and Ser 203. Nitrogen N3 of the imidazole ring of both enantiomers of compound **18** forms hydrogen bond with side chain oxygen of Ser 203. Aroyl phenyl ring and the corresponding cycloalkylamino groups are also found in the vicinity of oxyanion hole residues, Gly 121 and Gly 122. In Fig. 3c and d, the best docking poses, that belong to the most populated cluster, for the compounds **17** and **18** are shown. The orientation of the ligands is reversed, comparing to the energetically favored poses (Fig. 3a and b). Aroyl moieties of the ligands are accommodated at the entrance of the gorge (PAS), interacting with aromatic side chains of Trp 286 and Tyr 72. Phenylamido rings of the both compounds are directed toward the bottom of the AChE active site gorge and interact with the side chains of Tyr 337, Phe 338 and Trp 86 residues. The hydrogen bond between amido –NH– group and the side chain –OH of Tyr 124 is retained. The important difference between energetically favorable and the most populated docking poses for compounds **17** and **18** lies in the fact that ligands are found closer to the entrance of the gorge in the poses which belong to the most populated cluster. The upper part of the AChE active site gorge is wider, and can easily accommodate voluminous

diisopropyl-substituted aroyl groups of **17** and **18**, in a variety of slightly different, but essentially similar conformations. Most probably because of this, the search algorithm was able to find more similar poses belonging to the same cluster. One important consequence of this is that cycloalkylamino moieties of **17** and **18** are found near acyl pocket residues Phe 295 and Phe 297, instead near catalytic triad residues His 447 and Ser 203, as observed in the best ranked docking pose; therefore, in the most populated pose of **18**, N3 nitrogen of the imidazole ring forms hydrogen bond with backbone –NH– group of Phe 295. However, in both classes of poses, the hydrogen bond between amido –NH– group and side chain –OH group of Tyr 124 existed.

Docking poses of the both enantiomers of compound **6** are shown in Fig. 3e. Cluster which comprised the best ranked pose (according to the estimated  $\Delta G$  of binding) was also the most populated one. Both enantiomers were docked almost identically into the AChE active site gorge, and established the same type of interactions with amino acid side chains of the enzyme (see Table 2.). The estimated free energies of binding for the both enantiomers appeared very similar, –11.15 and –11.11 kcal/mol, for *S* and *R*, respectively. Phenylamide rings of both enantiomers are directed toward the bottom of the AChE active site gorge, and form hydrophobic interactions with aromatic side chains of Phe 338, Tyr 337 and Trp 86. The aroyl phenyl rings of the both *R* and *S* enantiomers are directed toward the entrance of the gorge, and interact with Tyr 72, Asp 74 and Trp 286 (residues that belong to PAS). Oxygen of the aroyl carbonyl group forms hydrogen bond with the backbone –NH– group of Phe 295. For this compound, only few poses (out of 50) were found with the aroyl phenyl ring directed toward bottom of the gorge, but with considerably lower estimated free energy of binding. So, when there are no voluminous 2,4-diisopropyl groups at aroyl moiety, which can establish important hydrophobic contact with the amino acid residues in the active site of AChE, and give rise to the energetically most favored (but poorly populated) docking poses (as in case of compounds **17** and **18**), the most populated pose becomes also the energetically favored one, with phenylamido moiety directed toward bottom of the gorge, and aroyl phenyl ring directed toward the entrance of the gorge.

The docking studies provided valuable insight into possible interactions between the three most active derivatives (**6**, **17** and **18**) and AChE active site residues. From exhaustive analysis of the docking poses it can be shown that there are two possible orientations of the ligands within the AChE active site gorge. One with aroyl moiety directed toward the bottom of the gorge, and the other with aroyl moiety directed toward the entrance of the gorge. The later one, in most of the solutions, belonged to the most populated cluster of conformations. Majority of the derivatives, in both classes of docking poses showed hydrogen bonding with Tyr 124 residue.

Protein flexibility was not accounted in our docking study. The knowledge on the non-covalent contacts between enzyme and ligand over time may provide additional information about most persistent interactions and the stability of the protein-ligand complexes. We performed the unconstrained, 10 ns molecular dynamics simulation, starting from the most populated docking pose of the *S* enantiomer of compound **18**. The movie, obtained from trajectory is given as Supplementary Material, Video 1. The most important distances between AChE active site residues and the ligand obtained from simulation are shown in Fig. 4. During the simulation, ligand moves toward the entrance of the gorge, as can be seen by a gradual increase of the distance between the centroid defined on the indole ring of Trp 86 and the phenylamido ring of compound **18** (4–~12 Å, Fig. 4a). After 5 ns, this distance remains stable until the end of the simulation. We also monitored the distance between aroyl ring of compound **18** and Trp 286 side chain

**Table 3**

Putative interactions of the selected compounds and AChE active site residues, obtained by docking calculations.

Comp. no <sup>a</sup>	Tyr 72	Asp 74	Trp 86 <sup>b</sup>	Gly 120	Gly 121	Gly 122	Tyr 124	Ser125	Tyr 133	Glu 202	Ser 203	Trp 286 <sup>b</sup>	Leu 289	Ser 293	Ile 294	Phe 295	Arg 296	Phe 297	Tyr 341	Tyr 337	Phe 338	His 447	ΔG
<b>2 (E, P)</b>	1	1	Ph	0	0	1	HB (NH) <sup>c</sup>	0	0	0	1	Ar	1	1	1	HB (CO)	1	1	1	1	1	HB (MeO)	–10.57
<b>6 (E, P)</b>	1	1	Ph	0	0	0	HB (NH)	0	0	1	0	Ar	1	1	1	HB (CO)	1	0	1	1	1	1	–11.15
<b>14 (E)</b>	1	1	Ph	1	1	1	HB (NH)	1	0	1	0	Ar	0	0	0	1	0	1	1	0	1	0	–9.67
<b>14 (P)</b>	1	1	Ar	0	0	0	HB (NH)	0	0	0	0	Ph	0	1	1	HB (Im)	HB (Im)	1	HB (NH)	1	1	0	–9.66
<b>17 (E)</b>	0	1	Ar	1	1	1	HB (NH)	1	1	0	1	Ph	0	1	1	0	1	1	1	1	1	1	–12.65
<b>17 (P)</b>	1	1	Ph	0	0	0	HB (NH)	0	0	1	0	Ar	0	0	1	1	1	1	1	1	1	1	–11.22
<b>18 (E)</b>	0	0	Ar	1	1	1	HB (NH)	1	1	1	0	Ph	1	1	1	1	1	1	0	1	1	1	–9.06
<b>18 (P)</b>	1	1	Ph	0	0	0	HB (NH)	0	0	1	0	Ar	0	0	1	HB (Im)	0	1	1	1	1	1	–8.96
<b>26 (E)</b>	1	1	Ar	0	1	1	HB (NH)	1	0	0	HB (Im)	Ph	0	1	1	HB (MeO)	1	1	0	1	1	1	–11.28
<b>26 (P)</b>	1	1	Ar	0	0	0	HB (NH)	0	0	0	0	Ph	0	0	1	HB (Im)	1	1	1	1	0	HB (MeO)	–10.76
<b>30 (E,P)</b>	1	1	Ph	0	0	0	HB (NH)	0	0	1	0	Ar	1	1	1	HB (CO)	1	1	1	1	1	1	–11.47
<b>2 (E)</b>	1	0	Ph	1	1	1	HB (NH)	1	1	0	HB (Im)	Ar	0	1	1	1	1	1	1	1	1	1	–10.39
<b>2 (P)</b>	1	1	Ph	0	0	0	HB (NH)	0	0	0	1	Ar	1	1	1	HB (CO)	1	1	1	1	1	1	–10.25
<b>6 (E, P)</b>	1	1	Ph	0	0	0	HB (NH)	0	0	1	0	Ar	1	1	1	HB (CO)	1	0	1	1	1	1	–11.11
<b>14 (E)</b>	1	1	Ph	0	0	1	HB (NH)	HB (MeO)	0	0	1	Ar	0	0	1	1	0	1	1	1	1	HB (Im)	–10.72
<b>14 (P)</b>	1	1	Ar	0	1	1	HB (NH)	1	0	0	1	Ph	0	0	1	HB (Im)	0	1	1	1	1	1	–9.42
<b>17 (E)</b>	0	1	Ar	1	1	1	HB (NH)	1	1	0	1	Ph	0	1	0	0	0	1	1	1	1	1	–10.92
<b>17 (P)</b>	1	1	Ph	0	1	0	HB (NH)	0	0	1	1	Ar	0	0	1	1	1	1	1	0	0	1	–10.89
<b>18 (E)</b>	0	0	Ar	1	1	1	HB (NH)	1	1	1	1	Ph	1	1	0	0	1	1	0	1	1	1	–10.62
<b>18 (P)</b>	1	1	Ph	0	0	0	HB (NH)	0	0	1	0	Ar	0	0	1	HB (Im)	0	1	1	1	1	1	–10.26
<b>26 (N, P)</b>	1	1	Ph	0	0	0	HB (NH)	0	0	0	1	Ar	1	1	1	1	1	1	1	1	1	HB (Im)	–11.00
<b>30 (E)</b>	1	1	Ar	0	1	1	HB (NH)	1	0	0	HB (Im)	Ph	0	1	1	1	1	1	0	1	1	HB (Im)	–11.62
<b>30 (P)</b>	1	1	Ar	0	1	0	HB (NH)	0	0	0	0	Ph	0	1	1	HB (Im)	0	0	1	1	0	1	–10.78

*Explanations:* The upper part of the table corresponds to the docking poses of *S* enantiomers, while lower part corresponds to docking poses of *R* enantiomers. The assignment '0' describes a lack of interaction between specified AChE residue and the ligand, while by '1', the presence of close contacts between ligand and AChE residue is indicated.

<sup>a</sup> The best ranked pose (E) and the most populated one (P), (E, P) – those poses are equal.

<sup>b</sup> In these columns is shown which moiety of the compounds interacts with AS (Trp 86) and PAS (Trp 286), assignment Ph corresponds to phenylamido moiety, and Ar to aroyl moiety of the molecules.

<sup>c</sup> The type of hydrogen bond (HB) that is formed between ligand and AChE active site residues is indicated: HB(NH) – between –NH– amide group and –OH group of Tyr 124 side chain; HB (MeO) – between methoxy group of the ligand and –OH group of Ser 125 side chain, or backbone –NH– group of Phe 295; HB(Im) – between imidazole nitrogen of the ligand and side chain –OH group of Ser 203, or backbone –NH– group of Phe 295; HB(CO) – between aroyl carbonyl group of the ligand and the backbone –NH– group of Phe 295.

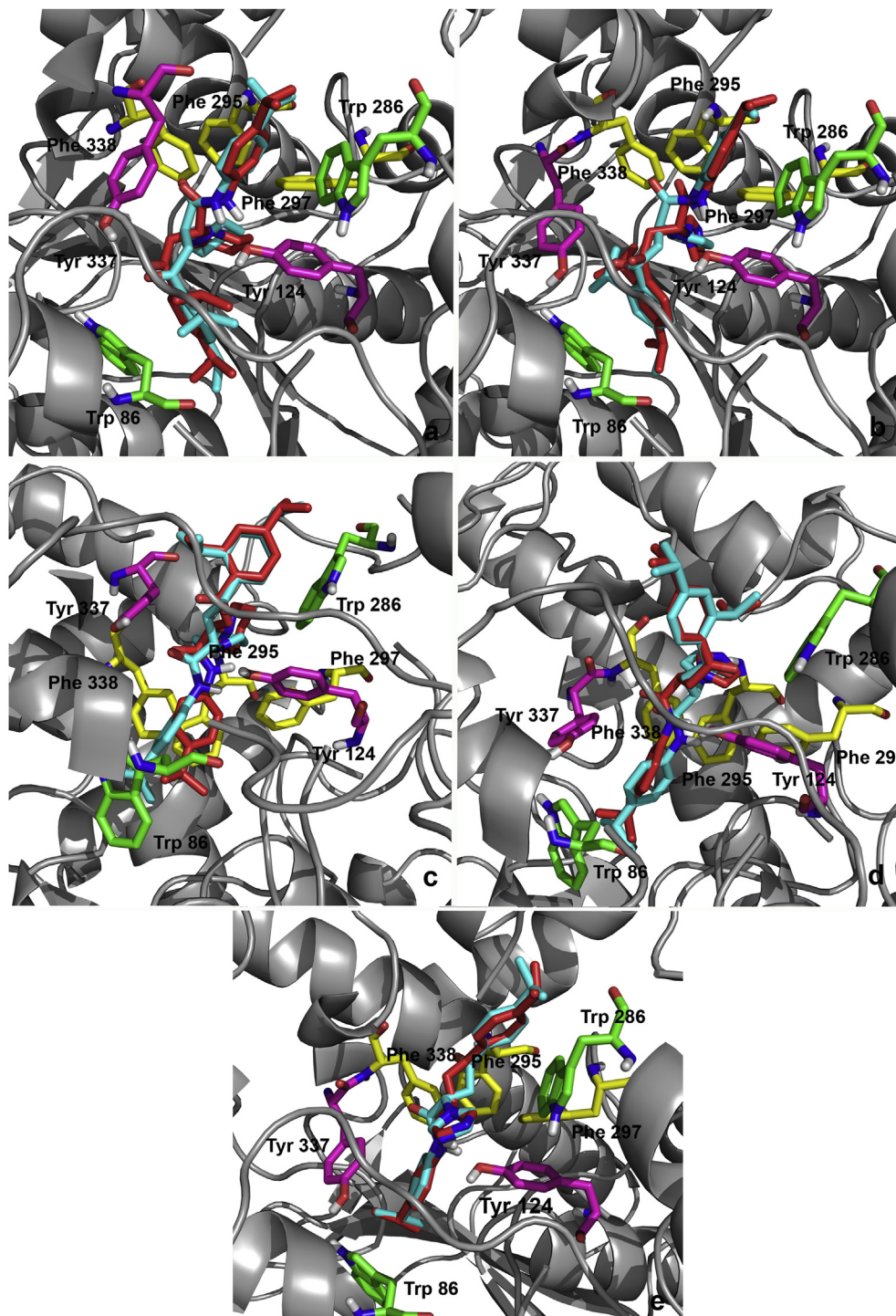


**Fig. 3.** Compounds **6**, **17** and **18** docked into the AChE active site. The *S* enantiomers are colored cyan and *R* enantiomers are colored red. (a) best ranked pose for **17**; (b) best ranked pose for **18**; (c) the most populated pose for **17**; (d) most populated pose for **18**; (e) best ranked/most populated pose for **6**. (For interpretation of the references to color in this figure legend, the reader is referred to the web version of this article.)

(PAS residue). A major fluctuation of the distance between centroids defined on Trp 286 indole ring and aryl phenyl moiety is observed during the first ns of the simulation (from 4.5 to almost 11 Å, Fig. 4b, blue squares). After this time, fluctuation of the distance appeared stable, with an average value of 7.5 Å. After 5 ns of simulation, the ligand rotates around the axis which passes through centroids defined on the aryl and on the phenylamido rings, so the distance gradually increases. We also monitored the distance

between methyl group of *ortho*-*i*-Pr moiety and centroid defined on the indole ring of Trp 286. The profile of this distance (Fig. 4b, violet dots) is similar to aryl-Trp 286 distance, and suggests a stable CH $\cdots\pi$  interaction with an average distance of 4 Å, from 1<sup>st</sup> to 5<sup>th</sup> ns of the trajectory. As a result of ligand rotation, this distance gradually increases from 5<sup>th</sup> ns to 8<sup>th</sup> ns, and after this time, remains stable with average value of 12 Å. Docking calculations suggested a hydrogen bond formation between backbone –NH–



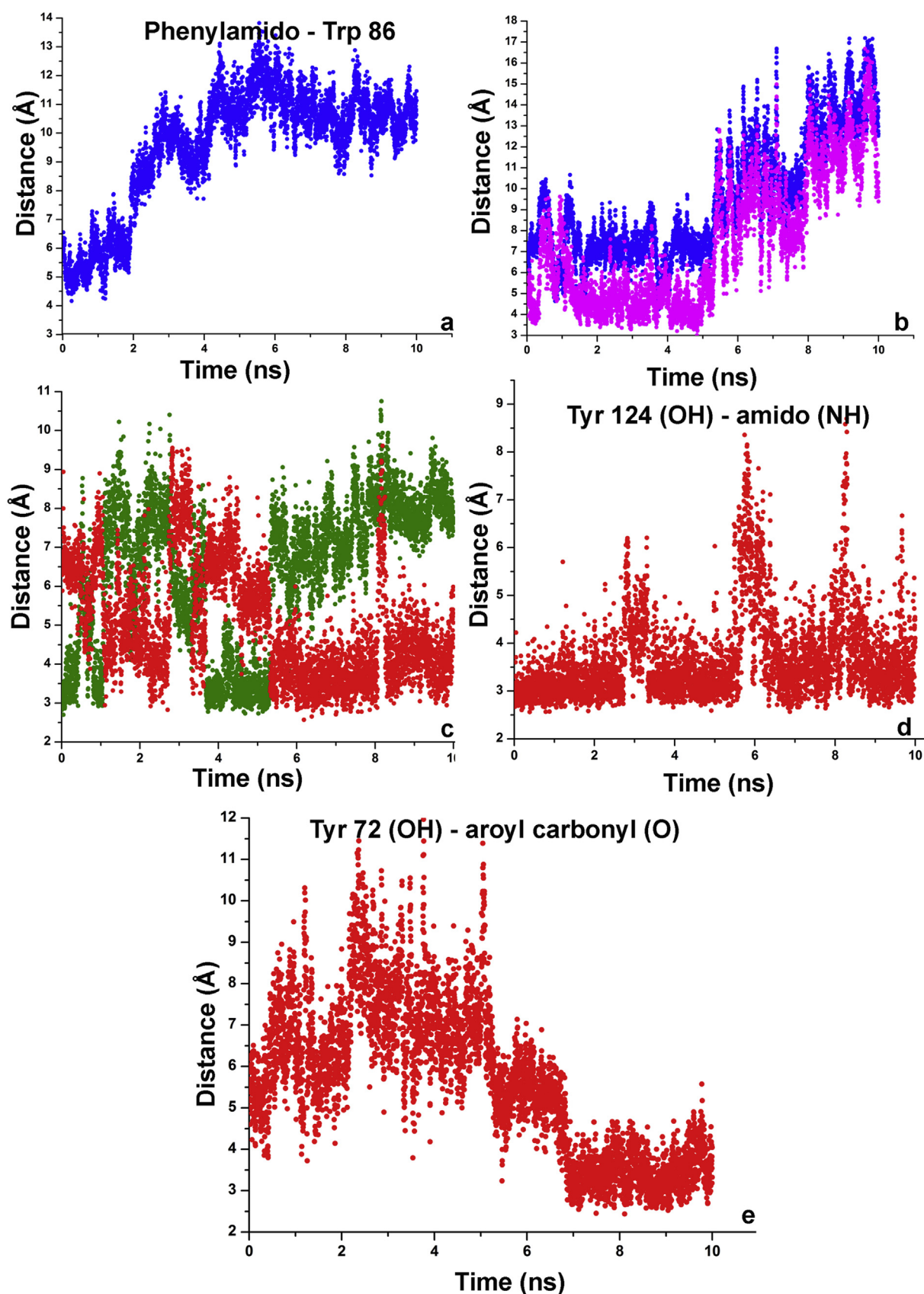


**Fig. 4.** The most important distances between AChE residues and compound **18** moieties, derived from the 10 ns of unconstrained MD: (a) Distance between centroids of phenylamide ring of **18** and Trp 82 aromatic side chain; (b) Blue squares—distance between centroids of aroyl ring and Trp 286 indole ring; violet dots — distance between centroid of Trp 286 indole ring and Me-group of *ortho-i*-Pr moiety; (c) Hydrogen bond between N3 of imidazole ring and: green dots — backbone —NH— group main chain nitrogen atom of Phe 295; red dots — —OH group oxygen of Tyr 124 (d) Distance between side chain —OH group oxygen of Tyr 124 and nitrogen atom of amido —NH— group; (e) distance between oxygen atom of Tyr 72 —OH group and carbonyl group of compound **18**. (For interpretation of the references to color in this figure legend, the reader is referred to the web version of this article.)



group of Phe 295 and the nitrogen N3 of the imidazole ring of compound **18**. We monitored this distance during simulation (Fig. 4c, green dots). This hydrogen bond appeared persistent only at the very beginning of the simulation, in the first 500 ps. From 1 ns to 4 ns of the simulation, the distance gradually increases. After 4 ns, the hydrogen bond between these two groups is formed again, and remains stable to the end of 5<sup>th</sup> ns. After this time, the bond breaks, as a result of ligand rotation. As a consequence of ligand rotation, imidazole ring is directed toward Tyr 124, and hydrogen bond is formed between the N3 of imidazole ring and the –OH group of Tyr 124 (Fig. 4c, red dots). The existence of this hydrogen bond is also evident from 500<sup>th</sup> ps to the end of 1<sup>st</sup> ns of the MD trajectory, the same time interval in which hydrogen bond of imidazole ring N3 and backbone –NH– group of Phe 295 cannot be observed. The distance between the side chain –OH oxygen atom of Tyr 124 and the amido –NH– of compound **18** is shown in Fig 4d. This H-bond remains stable throughout the whole 10 ns of MD simulation. Only temporary increase of this distance appeared around the 3<sup>rd</sup>, 6<sup>th</sup> and 8<sup>th</sup> ns of the simulation. Beyond that, the hydrogen bond is stable, with overall occupancy of 62.02%. One additional hydrogen bond was observed, between –OH group of Tyr 72 and carbonyl group of the ligand, from the 7<sup>th</sup> ns till the end of the simulation (Fig 4e). According to the results of this MD simulation, the most persistent, and therefore, probably, the most important interactions between compound **18** and the AChE active site residues involve following hydrogen bonds: persistent H-bond between Tyr 124 –OH group and amido –NH– moiety of the ligand; a fine interplay of hydrogen bonds between imidazole N3 atom of the compound and the Tyr 124 –OH group, or the backbone –NH– group of Phe 295; as well as the hydrogen bond between aroyl carbonyl group of compound and the Tyr 72 –OH group. Since the ligand moves slightly toward the entrance of the gorge, and therefore lose interactions with Trp 86 residue, we suppose that additional, more voluminous substituents in *para*-position of phenylamido moiety will increase the inhibition potency of compounds.

To explore possible binding modes for the compounds active toward BChE, and to reveal possible reasons for the selectivity of compounds toward one or another enzyme, we docked both enantiomers of compounds **16** and **20** into BChE active site (PDB entry 1P0I). The results are shown in Fig. 5, *S* enantiomers are colored cyan and *R* are colored red. The ligands occupy the same spatial region of the active site, and interact with BChE amino acid residues

primarily through hydrophobic interactions. The *S* and *R* enantiomers of compound **16** have slightly different modes of binding (Fig 5a). Aroyl phenyl ring of the *S* isomer of compound **16** is pointed toward the catalytic triad residues, His 438 and Ser 198. Aroyl carbonyl group forms hydrogen bond with Ser 198 –OH group. Phenylamido ring is found near anionic site of the enzyme, and forms close contact with Asn 83, while the amide bond of *S* enantiomer of compound **16** is found near Trp 82. The *N*-methyl group on the piperazine ring forms CH $\cdots\pi$  interaction with Trp 430 side chain. The orientation of the *R* enantiomer of compound **16** appeared slightly different. Aroyl phenyl ring is situated near Trp 82 residue. The *N*-methylpiperazine ring is pointed toward the entrance of the gorge and does not make any important interactions. The 3,5-dimethoxy substituted phenylamido ring is found near the Thr 120.

Both enantiomers of compound **20** have similar binding modes inside BChE active site (Fig. 5b). Phenylamido rings are found near catalytic triad residues His 438 and Ser 198. *N*-Methylpiperazine ring makes van der Waals interactions with Tyr 332 residue. Aroyl ring is situated in the anionic site of the enzyme, and forms hydrophobic interactions with Trp 82. The *ortho*-*i*-Pr group of aroyl ring forms close contacts with Gly 115, Gly 116 and Gly 117 (oxyanion hole residues). Any hydrogen bonding between enantiomers of compound **20** and the amino acid residues of BChE was not observed.

The binding modes of compounds **6**, **17** and **18** in the AChE active site are significantly different from the binding modes of compounds **16** and **20** in the BChE active site. As is mentioned in the introduction, six out of fourteen aromatic amino acid residues in AChE (Tyr 72, Tyr 124, Trp 286, Phe 295, Phe 297 and Tyr 337) are replaced by aliphatic ones (Asn 68, Gln 119, Ala 277, Leu 286, Val 288, and Ala 328) in BChE. This causes 200 Å<sup>3</sup> larger active site gorge of BChE, comparing to that of AChE. Most probably because of this, compounds **16** and **20** are deeply buried inside of BChE active side gorge, and oriented in way that two rings of the molecules are situated in the bottom of the gorge, one usually directed toward Trp 82 (anionic site) and the other toward Ser 198 and His 438 (catalytic triad residues). In contrast to this, compounds **6**, **17** and **18** are oriented in a way that one aromatic ring interacts with AS and the other one with PAS of AChE, with smaller cycloalkylamino moiety accommodated in the middle of the gorge. This binding mode is probably a consequence of the less voluminous AChE active site gorge comparing to BChE's. It is very probable that due to bulkiness

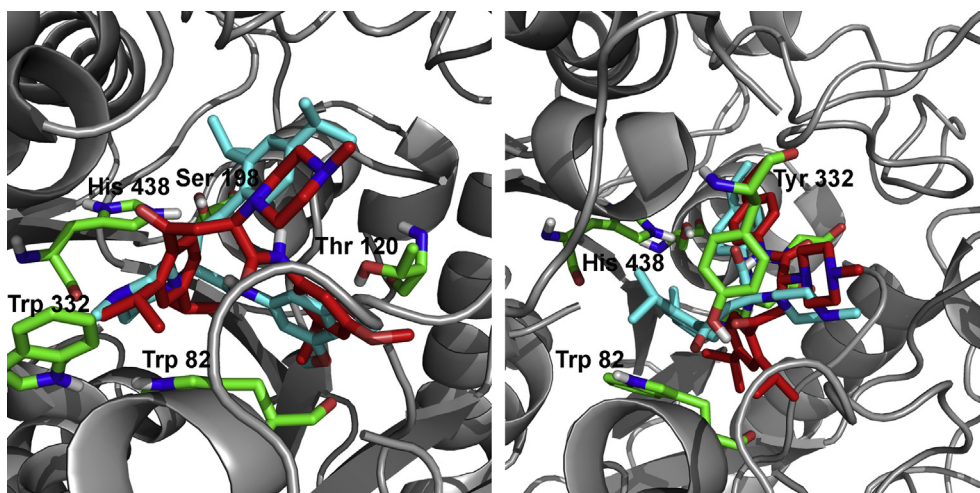


Fig. 5. Compounds **16** (left) and **20** (right) docked into the BChE active site. The *S* enantiomers are colored cyan and *R* enantiomers are colored red. (For interpretation of the references to color in this figure legend, the reader is referred to the web version of this article.)

of *N*-methylpiperazine ring (comparing to imidazole and piperidine ring), compounds **16** and **20** cannot be accommodated inside AChE active site, and therefore these compounds selectively inhibit BChE. Along with this, interactions of compounds **16** and **20** with BChE are primarily hydrophobic by nature (only one hydrogen bond is observed for compound **16**), while compound **18** establish few important hydrogen bonds with the Tyr 72 and the Tyr 124 residues of AChE; as perceived from MD simulation. Tyr 72 and the Tyr 124 residues are replaced with Asn 68 and Gln 119 in BChE. Therefore the architecture of the BChE active site is slightly different, comparing to AChE, and those residues cannot play the same role of hydrogen bond donors/acceptors as corresponding residues in AChE. Moreover, compounds **6**, **17**, **18** are less voluminous comparing to **16** and **20**, and probably cannot establish necessary hydrophobic contact in sufficient extent for the effective binding to the wider BChE active site gorge.

### 3. Conclusions

In continuation of our work, we further investigated influence of structural modifications of 4-aryl-4-oxo-2-aminybutyramides on AChE and BChE inhibition activity. We explored the influence of the amido part of molecules on the AChE/BChE inhibition activity and selectivity, changing the amido moiety from phenyl to 3,5-dimethoxyphenyl, 4-isopropylphenyl and cyclohexyl and keeping the favorable alkyl substituents (2,4-di-isopropyl, 4-isopropyl and  $\beta$ -tetralinyl) on the aryl part of the molecules. For the Michael addition to the activated double bond, piperidine, imidazole, morpholine, *N*-methylpiperazine, 4-benzylpiperidine and 4-(2-*N,N*-di-Me-aminoethyl)-1-piperazine were used. Twelve compounds, mostly piperidine and imidazolo derivatives, inhibited AChE in low micromolar range, and were inactive toward BChE. Three compounds inhibited BChE in low micromolar or submicromolar concentrations. All three compounds bear 2,4-diisopropyl substituted aryl moiety and a *N*-methylpiperazine ring at position C2 of butanoic part of molecule. As with previous set of compounds, the nature of cycloalkylamino moiety governed the AChE/BChE selectivity of the compounds. The most active AChE inhibitor, compound **17**, exhibited mixed type reversible inhibition, indicating its binding to free enzyme and enzyme–substrate complex. The docking study, performed with the seven derivatives having IC<sub>50</sub> values below 5  $\mu$ M, showed that for all compounds a hydrogen bond between amido –NH– group of compounds and Tyr 124 –OH group can be formed. The unconstrained, 10 ns molecular dynamics simulation of the complex between AChE and compound **18**, showed that most persistent ligand–protein interaction is hydrogen bond between Tyr 124 –OH group and amido –NH– moiety of compound. Few additional hydrogen bonds were also found. Although moderately active, reported compounds will be used as templates for further structural modifications, in order to find structural requirements needed for higher potency.

### 4. Experimental

#### 4.1. Chemistry

All chemicals were purchased from Sigma–Aldrich or Merck, and were used as received. Dry CH<sub>2</sub>Cl<sub>2</sub> was used for Friedel–Crafts acylations. Melting points were determined in open capillary tubes on SMP-10 Stuart apparatus, and are uncorrected. <sup>1</sup>H and <sup>13</sup>C NMR spectra were recorded in CDCl<sub>3</sub> on Varian Gemini 200/50 MHz or Bruker AVANCE 500/125 MHz instruments. NMR spectra of representative compounds are shown in Fig. S7, Supplementary Material. Chemical shifts are reported in parts per million (ppm) relative to tetramethylsilane (TMS) as internal standard. Spin multiplicities

are given as follows: *s* (singlet), *d* (doublet), *t* (triplet), *m* (multiplet), or *br* (broad). The HR ESI-MS spectra were recorded on Agilent Technologies 6210-1210 TOF-LC-ESI-MS instrument in positive mode. Samples were dissolved in MeOH. All compounds prove >98% purity, as obtained by instrumental methods of analysis.

#### 4.2. Characterization of the compounds 1–38

##### 4.2.1. *N*-(3,5-dimethoxyphenyl)-4-(4-isopropylphenyl)-4-oxo-2-(*R,S*)-(1-piperidinyl)butanamide (**1**)

C<sub>26</sub>H<sub>34</sub>N<sub>2</sub>O<sub>4</sub>, starting from (*E*)-4-(4-isopropylphenyl)-4-oxo-2-butenic acid (3,5-dimethoxyphenyl)amide (0.85 mmol) and a corresponding amount of piperidine, 0.179 g of **1** was obtained, 48.05% yield, light yellow solid, m.p. = 111–113 °C (toluene). <sup>1</sup>H NMR (200 MHz, CDCl<sub>3</sub>)  $\delta$ : 1.28 (*d*, 6H, *J* = 7.59 Hz, *i*-PrCH<sub>3</sub>); 1.47 (*m*, 2H, piperidinyl –CH<sub>2</sub>–); 1.63 (*m*, 4H, piperidinyl –CH<sub>2</sub>–); 2.57 (triplet-like, 4H, *J* = 5.16 Hz, piperidinyl –CH<sub>2</sub>–); 2.93–3.04 (overlapped *m*, 2H, *i*-PrCH and ABX); 3.66 (*dd*, 1H, *J*<sub>1,2</sub> = 6.37 Hz, *J*<sub>1,3</sub> = 9.40 Hz, ABX); 3.77 (*s*, 6H, –OCH<sub>3</sub>); 4.26 (*dd*, 1H, *J*<sub>1,2</sub> = 5.16 Hz, *J*<sub>1,3</sub> = 9.41 Hz, ABX); 6.22 (triplet-like, 1H, *J*<sub>1,2</sub> = 4.25 Hz, amido-*p*-phenyl); 6.79 (*s*, 1H, amido-*o*-phenyl); 6.80 (*s*, 1H, amido-*o*-phenyl); 7.33 (*d*, 2H, *J* = 8.50 Hz, aryl-*m*-phenyl); 7.97 (*d*, 2H, *J* = 8.50 Hz, aryl-*o*-phenyl); 9.47 (*s*, 1H, amido –NH–). <sup>13</sup>C NMR (50 MHz, CDCl<sub>3</sub>)  $\delta$ : 22.38; 22.58; 23.60; 23.87; 26.71; 31.85; 34.16; 44.48; 51.00; 55.35; 96.32; 97.36; 126.65; 128.51; 134.81; 139.61; 154.54; 161.04; 170.60; 198.22. ESI-MS HR: 439.2587 (*M*+1), Calc. 439.2597.

##### 4.2.2. *N*-(3,5-dimethoxyphenyl)-4-(4-isopropylphenyl)-4-oxo-2-(*R,S*)-(1-imidazolyl)butanamide (**2**)

C<sub>24</sub>H<sub>27</sub>N<sub>3</sub>O<sub>4</sub>, starting from (*E*)-4-(4-isopropylphenyl)-4-oxo-2-butenic acid (3,5-dimethoxyphenyl)amide (0.85 mmol) and a corresponding amount of imidazole, 0.249 g of **2** was obtained, 69.55% white solid, m.p. = 150–151 °C (toluene). <sup>1</sup>H NMR (200 MHz, CDCl<sub>3</sub>)  $\delta$ : 1.24 (*d*, 6H, *J* = 6.71 Hz, *i*-PrCH<sub>3</sub>); 2.93 (*m*, 1H, *J*<sub>1,2</sub> = 7.05 Hz, *J*<sub>1,3</sub> = 14.11 Hz, *i*-Pr-CH); 3.50 (*dd*, 1H, *J*<sub>1,2</sub> = 5.64 Hz, *J*<sub>1,3</sub> = 18.11 Hz, ABX); 3.66 (*s*, 6H, –OCH<sub>3</sub>); 4.08 (*dd*, 1H, *J*<sub>1,2</sub> = 7.29 Hz, *J*<sub>1,3</sub> = 18.11 Hz, ABX); 5.66 (*t*, 1H, *J*<sub>1,2</sub> = 6.35 Hz, ABX); 6.18 (triplet-like, 1H, *J*<sub>1,2</sub> = 2.35 Hz, amido-*p*-phenyl); 6.81 (*s*, 1H, amido-*o*-phenyl); 6.82 (*s*, 1H, amido-*o*-phenyl); 7.16 (*s*, 1H, imidazolyl –CH–); 7.21 (*s*, 1H, imidazolyl –CH–); 7.26 (*d*, 2H, *J* = 8.00 Hz aryl-*m*-phenyl); 7.64 (*s*, 1H, imidazolyl –CH–); 7.84 (*d*, 2H, *J* = 7.86, Hz aryl-*o*-phenyl); 10.30 (*s*, 1H, amido –NH–). <sup>13</sup>C NMR (50 MHz, CDCl<sub>3</sub>)  $\delta$ : 23.49; 34.20; 41.73; 55.19; 56.75; 97.17; 98.12; 118.04; 126.83; 128.42; 129.44; 133.57; 137.41; 139.70; 155.60; 160.86; 166.56; 195.84. ESI-MS HR: 422.2074 (*M*+1), Calc. 422.2080.

##### 4.2.3. *N*-(3,5-dimethoxyphenyl)-4-(4-isopropylphenyl)-4-oxo-2-(*R,S*)-(4-morpholinyl)butanamide (**3**)

C<sub>25</sub>H<sub>32</sub>N<sub>2</sub>O<sub>5</sub>, starting from (*E*)-4-(4-isopropylphenyl)-4-oxo-2-butenic acid (3,5-dimethoxyphenyl)amide (0.82 mmol) and a corresponding amount of morpholine, 0.275 g of **3** was obtained, 76.01% yield, light yellow solid, m.p. = 155–157 °C (toluene). <sup>1</sup>H NMR (200 MHz, CDCl<sub>3</sub>)  $\delta$ : 1.27 (*d*, 6H, *J* = 7.46 Hz, *i*-PrCH<sub>3</sub>); 2.64 (triplet-like, 4H, *J*<sub>1,2</sub> = 4.00 Hz, morpholino –CH<sub>2</sub>–); 2.90–3.04 (overlapped *m*, 2H, *i*-PrCH and ABX); 3.64–3.86 (overlapped *m*, 11H, morpholino –CH<sub>2</sub>–, ABX and –OCH<sub>3</sub>); 4.27 (*dd*, 1H, *J*<sub>1,2</sub> = 5.14 Hz, *J*<sub>1,3</sub> = 7.14 Hz, ABX); 6.23 (triplet-like, 1H, *J*<sub>1,2</sub> = 2.82 Hz, amido-*p*-phenyl); 6.78 (*s*, 1H, amido-*o*-phenyl); 6.79 (*s*, 1H, amido-*o*-phenyl); 7.33 (*d*, 2H, *J* = 8.46 Hz, aryl-*m*-phenyl); 7.96 (*d*, 2H, *J* = 7.81 Hz, aryl-*o*-phenyl); 9.22 (*s*, 1H, amido –NH–). <sup>13</sup>C NMR (50 MHz, CDCl<sub>3</sub>)  $\delta$ : 23.54; 32.10; 34.14; 49.96; 55.30; 65.02; 67.30; 96.45; 97.46; 129.69; 128.45; 134.59; 139.34; 157.74; 161.04; 169.73; 197.74. ESI-MS HR: 441.2389 (*M*+1), Calc. 441.2389.

#### 4.2.4. *N*-(3,5-dimethoxyphenyl)-4-(4-isopropylphenyl)-4-oxo-2-(*R,S*)-[1-(4-methylpiperazinyl)]-butanamide (**4**)

C<sub>26</sub>H<sub>35</sub>N<sub>3</sub>O<sub>4</sub>, starting from (*E*)-4-(4-isopropylphenyl)-4-oxo-2-butenic acid (3,5-dimethoxyphenyl)amide (0.82 mmol) and a corresponding amount of 4-methylpiperazine, 0.159 g of **4** was obtained, 42.68% yield, white solid, m.p. = 120–122 °C (toluene). <sup>1</sup>H NMR (200 MHz, CDCl<sub>3</sub>) δ: 1.27 (d, 6H, *J* = 7.36 Hz, *i*-PrCH<sub>3</sub>); 2.32 (s, 3H, *N*-CH<sub>3</sub>); 2.52 (br, 4H, piperazine –CH<sub>2</sub>–); 2.67 (br, 4H, piperazine –CH<sub>2</sub>–); 2.93–3.08 (overlapped *m*, 2H, ABX and *i*-PrCH<sub>3</sub>); 3.63–3.77 (overlapped signals, 7H, ABX and –OCH<sub>3</sub>); 4.34 (dd, 1H, *J*<sub>1,2</sub> = 5.10 Hz, *J*<sub>1,3</sub> = 6.86 Hz, ABX); 6.23 (br, 1H, amido-*p*-phenyl); 6.79 (s, 1H, amido-*o*-phenyl); 6.80 (s, 1H, amido-*o*-phenyl); 7.32 (d, 2H, *J* = 8.43, aryl-*m*-phenyl); 7.96 (d, 2H, *J* = 8.43, aryl-*o*-phenyl); 9.30 (s, 1H, amido –NH–). <sup>13</sup>C NMR (50 MHz, CDCl<sub>3</sub>) δ: 23.58; 31.72; 34.16; 45.88; 55.33; 64.56; 96.28; 97.43; 126.65; 128.47; 134.70; 139.49; 154.63; 161.04; 170.04; 197.80. ESI-MS HR: 454.2707 (M+1), Calc. 454.2706.

#### 4.2.5. *N*-(4-isopropylphenyl)-4-(4-isopropylphenyl)-4-oxo-2-(*R,S*)-(1-piperidinyl)butanamide (**5**)

C<sub>27</sub>H<sub>36</sub>N<sub>2</sub>O<sub>2</sub>, starting from (*E*)-4-(4-isopropylphenyl)-4-oxo-2-butenic acid (4-isopropylphenyl)amide (0.74 mmol) and a corresponding amount of piperidine, 0.188 g of **5** was obtained, 59.90% yield, light yellow solid, m.p. = 106–108 °C (toluene). <sup>1</sup>H NMR (200 MHz, CDCl<sub>3</sub>) δ: 1.22 (d, 6H, *J* = 7.30 Hz, *i*-PrCH<sub>3</sub>–phenylamide); 1.27 (d, 6H, *J* = 7.30 Hz, *i*-PrCH<sub>3</sub>–aroyl); 1.46 (m, 2H, piperidinyl –CH<sub>2</sub>–); 1.63 (m, 4H, piperidinyl –CH<sub>2</sub>–); 2.57 (m, 4H, piperidinyl –CH<sub>2</sub>–); 2.83–3.00 (overlapped *m*, 3H, *i*-PrCH and ABX); 3.71 (dd, 1H, *J*<sub>1,2</sub> = 6.74 Hz, *J*<sub>1,3</sub> = 16.18 Hz, ABX); 4.26 (t, 1H, *J*<sub>1,2</sub> = 5.62 Hz, ABX); 7.16 (d, 2H, *J* = 7.86 Hz, amido-*m*-phenyl); 7.32 (d, 2H, *J* = 7.86 Hz, aryl-*m*-phenyl); 7.46 (d, 2H, *J* = 8.41 Hz, amido-*o*-phenyl); 7.97 (d, 2H, *J* = 7.86 Hz, aryl-*o*-phenyl); 9.39 (s, 1H, amido –NH–). <sup>13</sup>C NMR (50 MHz, CDCl<sub>3</sub>) δ: 23.58; 23.94; 26.69; 31.87; 33.49; 34.14; 51.02; 66.78; 95.70; 119.31; 126.61; 126.76; 128.49; 134.95; 135.55; 144.55; 154.38; 170.38; 198.37. ESI-MS HR: 421.2838 (M+1), Calc. 421.2855.

#### 4.2.6. *N*-(4-isopropylphenyl)-4-(4-isopropylphenyl)-4-oxo-2-(*R,S*)-(1-imidazolyl)butanamide (**6**)

C<sub>25</sub>H<sub>29</sub>N<sub>3</sub>O<sub>2</sub>, starting from (*E*)-4-(4-isopropylphenyl)-4-oxo-2-butenic acid (4-isopropylphenyl)amide (0.74 mmol) and a corresponding amount of imidazole, 0.251 g of **6** was obtained, 83.35% yield, white solid, m.p. = 164–165 °C (toluene). <sup>1</sup>H NMR (200 MHz, CDCl<sub>3</sub>) δ: 1.17 (d, 6H, *J* = 7.45 Hz, *i*-PrCH<sub>3</sub>–phenylamide); 1.24 (d, 6H, *J* = 6.09 Hz, *i*-PrCH<sub>3</sub>–aroyl); 2.75–3.01 (overlapped *m*, 2H, *i*-PrCH<sub>3</sub>); 3.49 (dd, 1H, *J*<sub>1,2</sub> = 5.65 Hz, *J*<sub>1,3</sub> = 18.12 Hz, ABX); 4.10 (dd, 1H, *J*<sub>1,2</sub> = 7.13 Hz, *J*<sub>1,3</sub> = 17.24 Hz, ABX); 5.65 (t, 1H, *J*<sub>1,2</sub> = 6.24 Hz, ABX); 7.09 (d, 2H, *J* = 8.48 Hz, amido-*m*-phenyl); 7.14 (s, 1H, imidazolyl-CH); 7.21 (s, 1H, imidazolyl-CH); 7.27 (d, 2H, *J* = 8.47, aryl-*m*-phenyl); 7.45 (d, 2H, *J* = 8.48 Hz, amido-*o*-phenyl); 7.62 (s, 1H, imidazolyl-CH); 7.85 (d, 2H, *J* = 8.47, aryl-*o*-phenyl); 9.97 (s, 1H, amido –NH–). <sup>13</sup>C NMR (50 MHz, CDCl<sub>3</sub>) δ: 22.53; 23.91; 33.50; 34.21; 41.75; 56.68; 95.73; 118.02; 120.19; 126.76; 128.42; 129.55; 133.66; 135.50; 137.41; 145.31; 155.53; 166.36; 195.82. ESI-MS HR: 404.2337 (M+1), Calc. 404.2338.

#### 4.2.7. *N*-(4-isopropylphenyl)-4-(4-isopropylphenyl)-4-oxo-2-(*R,S*)-(4-morpholinyl)butanamide (**7**)

C<sub>26</sub>H<sub>34</sub>N<sub>2</sub>O<sub>3</sub>, starting from (*E*)-4-(4-isopropylphenyl)-4-oxo-2-butenic acid (4-isopropylphenyl)amide (0.89 mmol) and a corresponding amount of morpholine, **7** was obtained, in quantitative yield, as yellow semi-solid. <sup>1</sup>H NMR (200 MHz, CDCl<sub>3</sub>) δ: 1.22 (d, 6H, *J* = 6.69 Hz, *i*-PrCH<sub>3</sub>–phenylamide); 1.26 (d, 6H, *J* = 7.31 Hz, *i*-PrCH<sub>3</sub>–aroyl); 2.64 (triplet-like, 4H, *J* = 4.26 Hz morpholinyl –CH<sub>2</sub>–); 2.79–3.06 (overlapped *m*, 3H, ABX and *i*-Pr-CH); 3.66–3.77

(overlapped *m*, 5H, ABX and morpholinyl –CH<sub>2</sub>–); 4.27 (dd, 1H, *J*<sub>1,2</sub> = 5.18 Hz, *J*<sub>1,3</sub> = 9.44 Hz, ABX); 7.16 (d, 2H, *J* = 8.83 Hz, amido-*m*-phenyl); 7.31 (d, 2H, *J* = 7.62, aryl-*m*-phenyl); 7.44 (d, 2H, *J* = 8.22 Hz, amido-*o*-phenyl); 7.96 (d, 2H, *J* = 8.52, aryl-*o*-phenyl); 9.16 (s, 1H, amido –NH–). <sup>13</sup>C NMR (50 MHz, CDCl<sub>3</sub>) δ: 23.56; 23.93; 32.14; 33.47; 34.16; 50.00; 65.15; 67.31; 95.70; 119.44; 126.69; 126.83; 128.49; 135.24; 144.89; 154.69; 169.55; 197.86. ESI-MS HR: 423.2642 (M+1), Calc. 423.2648.

#### 4.2.8. *N*-(4-isopropylphenyl)-4-(4-isopropylphenyl)-4-oxo-2-(*R,S*)-[1-(4-methylpiperazinyl)]butanamide (**8**)

C<sub>27</sub>H<sub>37</sub>N<sub>3</sub>O<sub>2</sub>, starting from (*E*)-4-(4-isopropylphenyl)-4-oxo-2-butenic acid (4-isopropylphenyl)amide (0.89 mol) and a corresponding amount of 1-methylpiperazine, 0.145 g of **8** was obtained, in quantitative yield, as yellow semi-solid. <sup>1</sup>H NMR (200 MHz, CDCl<sub>3</sub>) δ: 1.22 (d, 6H, *J* = 7.01 Hz, *i*-PrCH<sub>3</sub>–phenylamide); 1.26 (d, 6H, *J* = 7.01 Hz, *i*-PrCH<sub>3</sub>–aroyl); 2.31 (s, 3H, piperazine-CH<sub>3</sub>); 2.87 (m, 1H, *J*<sub>1,2</sub> = 6.72 Hz, *J*<sub>1,3</sub> = 13.83 Hz, *i*-PrCH); 2.87 (overlapped *m*, 2H, ABX and *i*-PrCH); 2.53 (br, 4H, piperazine –CH<sub>2</sub>–); 2.68 (br, 4H, piperazine –CH<sub>2</sub>–); 3.70 (dd, 1H, *J*<sub>1,2</sub> = 7.29 Hz, *J*<sub>1,3</sub> = 16.34 Hz, ABX); 4.33 (triplet-like picks, *J*<sub>1,2</sub> = 7.04 Hz, ABX); 7.16 (d, 2H, *J* = 8.30 Hz, amido-*m*-phenyl); 7.31 (d, 2H, *J* = 8.30, aryl-*m*-phenyl); 7.45 (d, 2H, *J* = 8.80 Hz, amido-*o*-phenyl); 7.95 (d, 2H, *J* = 8.05, aryl-*o*-phenyl); 9.21 (s, 1H, amido –NH–). <sup>13</sup>C NMR (50 MHz, CDCl<sub>3</sub>) δ: 26.63; 23.99; 31.87; 33.55; 34.22; 45.94; 55.62; 64.80; 119.40; 126.66; 126.82; 128.50; 134.87; 135.41; 144.78; 154.54; 169.81; 198.01. ESI-MS HR: 436.2965 (M+1), Calc. 436.2964.

#### 4.2.9. *N*-cyclohexyl-4-(4-isopropylphenyl)-4-oxo-2-(*R,S*)-(1-piperidinyl)butanamide (**9**)

C<sub>24</sub>H<sub>36</sub>N<sub>2</sub>O<sub>2</sub>, starting from (*E*)-4-(4-isopropylphenyl)-4-oxo-2-butenic acid cyclohexylamide (0.83 mmol) and a corresponding amount of piperidine, 0.160 g of **9** was obtained, 49.74% yield, yellow semi-solid. <sup>1</sup>H NMR (200 MHz, CDCl<sub>3</sub>) δ: 1.25 (d, 6H, *J* = 6.71 Hz, *i*-PrCH<sub>3</sub>); 1.14–1.45 (overlapped *m*, 8H, cyclohexyl –CH<sub>2</sub>–, piperidinyl –CH<sub>2</sub>–); 1.54–1.66 (overlapped *m*, 6H, cyclohexyl –CH<sub>2</sub>–, piperidinyl –CH<sub>2</sub>–); 1.78–3.77 (br, 2H, cyclohexyl –CH<sub>2</sub>–); 2.50 (triplet-like picks, 4H, *J* = 5.97 Hz, piperidinyl –CH<sub>2</sub>–); 2.84 (dd, 1H, *J*<sub>1,2</sub> = 5.11 Hz, *J*<sub>1,3</sub> = 16.48 Hz, ABX); 2.95 (m, 1H, *i*-PrCH); 3.63 (dd, 1H, *J*<sub>1,2</sub> = 7.39 Hz, *J*<sub>1,3</sub> = 16.19 Hz, ABX); 3.77 (m, 1H, cyclohexyl –CH–); 4.06 (dd, 1H, *J*<sub>1,2</sub> = 5.69 Hz, *J*<sub>1,3</sub> = 9.66 Hz, ABX); 7.30 (d, 2H, *J* = 7.96 Hz, aryl-*m*-phenyl); 7.95 (d, 2H, *J* = 8.24 Hz, aryl-*o*-phenyl); 6.83 (d, 1H, *J* = 13.14 Hz, amido –NH–); <sup>13</sup>C NMR (50 MHz, CDCl<sub>3</sub>) δ: 23.58; 24.02; 24.60; 25.49; 26.60; 32.05; 32.90; 33.12; 34.14; 47.50; 50.91; 65.58; 126.56; 128.47; 135.26; 154.14; 171.06. ESI-MS HR: 385.2855 (M+1), Calc. 385.2842.

#### 4.2.10. *N*-cyclohexyl-4-(4-isopropylphenyl)-4-oxo-2-(*R,S*)-(1-imidazolyl)butanamide (**10**)

C<sub>22</sub>H<sub>29</sub>N<sub>3</sub>O<sub>2</sub>, starting from (*E*)-4-(4-isopropylphenyl)-4-oxo-2-butenic acid cyclohexylamide (0.83 mol) and a corresponding amount of imidazole, 0.148 g of **10** was obtained, 48.14% yield, orange semi-solid. <sup>1</sup>H NMR (200 MHz, CDCl<sub>3</sub>) δ: 1.06–1.41 (m, 6H, cyclohexyl –CH<sub>2</sub>–); 1.25 (d, 6H, *J* = 7.28 Hz, *i*-PrCH<sub>3</sub>); 1.61 (m, 2H, cyclohexyl –CH<sub>2</sub>–); 1.83 (br, 2H, cyclohexyl –CH<sub>2</sub>–); 2.95 (m, 1H, *i*-PrCH); 3.49 (dd, 1H, *J*<sub>1,2</sub> = 6.68 Hz, *J*<sub>1,3</sub> = 17.91 Hz, ABX); 3.72 (m, 1H, cyclohexyl –CH–); 4.02 (dd, 1H, *J*<sub>1,2</sub> = 6.67 Hz, *J*<sub>1,3</sub> = 17.90 Hz, ABX); 5.45 (triplet-like picks, 1H, *J*<sub>1,2</sub> = 6.68 Hz, ABX); 6.65 (d, 1H, *J* = 7.86 Hz, amido-NH); 7.07 (s, 1H, imidazolyl-CH); 7.12 (s, 1H, imidazolyl-CH); 7.30 (d, 2H, *J* = 8.50 Hz, aryl-*m*-phenyl); 7.71 (s, 1H, imidazolyl-CH); 7.86 (d, 2H, *J* = 8.49 Hz, aryl-*o*-phenyl); <sup>13</sup>C NMR (50 MHz, CDCl<sub>3</sub>) δ: 23.51; 24.60; 25.24; 32.48; 34.20; 41.61; 48.82; 56.39; 117.97; 126.81; 128.36; 129.31; 133.75; 137.28;

155.47; 167.34; 195.67. ESI-MS HR: 368.2336 ( $M+1$ ), Calc. 368.2338.

#### 4.2.11. *N*-cyclohexyl-4-(4-isopropylphenyl)-4-oxo-2-(*R,S*)-(4-morpholinyl)butanamide (**11**)

$C_{23}H_{34}N_2O_3$ , starting from (*E*)-4-(4-isopropylphenyl)-4-oxo-2-butenic acid cyclohexylamide (0.94 mmol) and a corresponding amount of morpholine, 0.131 g of **11** was obtained, 35.92% yield, pale orange solid, m.p. = 93–95 °C (toluene).  $^1H$  NMR (200 MHz,  $CDCl_3$ )  $\delta$ : 1.09 (*br*, 6H, cyclohexyl  $-CH_2-$ ); 1.26 (*d*, 6H,  $J$  = 11.26 Hz, *i*-Pr $CH_3$ ); 1.64 (*br*, 2H, cyclohexyl  $-CH_2-$ ); 1.86 (*br*, 2H, cyclohexyl  $-CH_2-$ ); 2.58 (*t*, 4H,  $J_{1,2}$  = 4.57 Hz, morpholino  $-CH_2-$ ); 2.86–2.99 (overlapped *m*, 2H, *i*-PrCH and ABX); 3.59–3.76 (overlapped *m*, 6H, ABX, morpholino  $-CH_2-$ , and cyclohexyl  $-CH-$ ); 4.07 (*dd*, 1H,  $J_{1,2}$  = 5.10 Hz,  $J_{1,3}$  = 7.84 Hz, ABX); 7.05 (*d*, 1H,  $J$  = 7.84 Hz, amido  $-NH-$ ); 7.31 (*d*, 2H,  $J$  = 8.43, aroyl-*m*-phenyl); 7.94 (*d*, 2H,  $J$  = 8.43, aroyl-*o*-phenyl).  $^{13}C$  NMR (50 MHz,  $CDCl_3$ )  $\delta$ : 23.60; 24.66; 25.46; 32.43; 32.92; 33.21; 34.20; 47.74; 50.02; 64.97; 67.31; 126.67; 128.47; 135.01; 154.49; 170.20; 198.31. ESI-MS HR: 387.2639 ( $M+1$ ), Calc. 387.2648.

#### 4.2.12. *N*-cyclohexyl-4-(4-isopropylphenyl)-4-oxo-2-(*R,S*)-[1-(4-methylpiperazinyl)butanamide (**12**)

$C_{24}H_{37}N_3O_2$ , starting from (*E*)-4-(4-isopropylphenyl)-4-oxo-2-butenic acid cyclohexylamide (0.83 mmol) and a corresponding amount of 1-methylpiperazine, 0.045 g of **12** was obtained, 13.46% yield, yellow solid, m.p. = 101–103 °C (toluene).  $^1H$  NMR (200 MHz,  $CDCl_3$ )  $\delta$ : 1.12–1.39 (*br*, 6H, cyclohexyl  $-CH_2-$ ); 1.25 (*d*, 6H,  $J$  = 6.97 Hz, *i*-Pr $CH_3$ ); 1.56–1.64 (*br*, 2H, cyclohexyl  $-CH_2-$ ); 1.86 (*br*, 2H, cyclohexyl  $-CH_2-$ ); 2.30 (*s*, 3H,  $-N-CH_3$ ); 2.42–2.51 (*br*, 4H, piperazine  $-CH_2-$ ); 2.60 (doublet-like, 4H, piperazine  $-CH_2-$ ); 2.83–2.99 (overlapped *m*, 2H, *i*-Pr-CH, ABX); 3.63 (*dd*, 1H,  $J_{1,2}$  = 7.94 Hz,  $J_{1,3}$  = 16.21 Hz, ABX); 3.77 (*br*, 1H, cyclohexyl  $-CH-$ ); 4.14 (*dd*, 1H,  $J_{1,2}$  = 5.16 Hz,  $J_{1,3}$  = 8.44 Hz, ABX); 7.11 (doublet-like, 1H,  $J$  = 8.21 Hz, amido-NH); 7.30 (*d*, 2H,  $J$  = 8.44 Hz, aroyl-*m*-phenyl); 7.93 (*d*, 2H,  $J$  = 8.44 Hz, aroyl-*o*-phenyl);  $^{13}C$  NMR (50 MHz,  $CDCl_3$ )  $\delta$ : 23.56; 24.58; 25.42; 31.90; 32.87; 33.14; 34.12; 45.81; 47.56; 55.42; 64.51; 126.54; 128.42; 135.06; 154.25; 170.40; 198.48. ESI-MS HR: 400.2959 ( $M+1$ ), Calc. 400.2964.

#### 4.2.13. 4-(2,4-Diisopropylphenyl)-*N*-(3,5-dimethoxyphenyl)-4-oxo-2-(*R,S*)-(1-piperidinyl)butanamide (**13**)

$C_{29}H_{40}N_2O_4$ , starting from (*E*)-4-(2,4-diisopropylphenyl)-4-oxo-2-butenic acid (3,5-dimethoxyphenyl)amide (0.76 mol) and a corresponding amount of piperidine, **13** was obtained, in quantitative yield, orange solid, m.p. = 99–101 °C (toluene).  $^1H$  NMR (500 MHz,  $CDCl_3$ )  $\delta$ : 1.21–1.29 (overlapped *m*, 12H, *i*-Pr $CH_3$ ); 1.52 (*m*, 2H, piperidino  $-CH_2-$ ); 1.66 (*m*, 4H, piperidino  $-CH_2-$ ); 2.55 (*m*, 4H, piperidino  $-CH_2-$ ); 2.87–2.96 (overlapped *m*, 2H, *i*-PrCH and ABX); 3.45–3.52 (overlapped *m*, 2H, *i*-PrCH and ABX); 3.77 (*s*, 6H,  $-OCH_3$ ); 4.20 (*dd*, 1H,  $J_{1,2}$  = 4.69 Hz,  $J_{1,3}$  = 8.04 Hz, ABX); 6.22 (*t*, 1H,  $J$  = 2.07 Hz, amido-*p*-phenyl); 6.79 (*s*, 2H, amido-*o*-phenyl); 7.26–7.27 (overlapped *d* and *s*, 2H, aroyl-*m*-phenyl); 7.63 (*d*, 1H,  $J$  = 7.79 Hz, aroyl-*o*-phenyl); 9.37 (*s*, 1H, amido  $-NH-$ ).  $^{13}C$  NMR (125 MHz,  $CDCl_3$ )  $\delta$ : 22.85; 23.16; 23.75; 23.95; 24.42; 26.73; 29.13; 34.26; 35.99; 44.50; 55.35; 66.27; 96.37; 97.39; 98.68; 123.16; 124.72; 127.97; 136.51; 139.64; 148.34; 152.00; 161.05; 170.57; 203.13. ESI-MS HR: 481.3075 ( $M+1$ ), Calc. 481.3066.

#### 4.2.14. 4-(2,4-Diisopropylphenyl)-*N*-(3,5-dimethoxyphenyl)-4-oxo-2-(*R,S*)-(1-imidazolyl)butanamide (**14**)

$C_{27}H_{33}N_3O_4$ , starting from (*E*)-4-(2,4-diisopropylphenyl)-4-oxo-2-butenic acid (3,5-dimethoxyphenyl)amide (0.89 mmol) and a corresponding amount of imidazole, 0.220 g of **14** was obtained, 52.94% yield, orange solid, m.p. = 103–105 °C (toluene).  $^1H$  NMR

(200 MHz,  $CDCl_3$ )  $\delta$ : 1.11–1.26 (overlapped *m*, 12H, *i*-Pr $CH_3$ ); 2.91 (*m*, 1H,  $J_{1,2}$  = 8.69 Hz,  $J_{1,3}$  = 14.28 Hz, *i*-Pr-CH); 3.31–3.50 (overlapped *m*, 2H, *i*-PrCH and ABX); 3.68 (*s*, 6H,  $-OCH_3$ ); 3.98 (*dd*, 1H,  $J_{1,2}$  = 7.45 Hz,  $J_{1,3}$  = 18.25 Hz, ABX); 5.66 (*t*, 1H,  $J_{1,2}$  = 7.19 Hz, ABX); 6.20 (*br*, 1H, amido-*p*-phenyl); 6.81 (*s*, 1H, amido-*m*-phenyl); 6.82 (*s*, 1H, amido-*m*-phenyl); 7.01–7.10 (overlapped signals, 2H, aroyl-*m*-phenyl); 7.17 (*s*, 1H, imidazolyl  $-CH-$ ); 7.24 (*s*, 1H, imidazolyl  $-CH-$ ); 7.48 (*d*, 1H,  $J$  = 8.39, aroyl-*o*-phenyl); 7.70 (*s*, 1H, imidazolyl  $-CH-$ ); 9.85 (*s*, 1H, amido  $-NH-$ ).  $^{13}C$  NMR (50 MHz,  $CDCl_3$ )  $\delta$ : 23.62; 23.96; 28.99; 34.27; 45.08; 55.24; 57.19; 97.21; 98.30; 117.97; 123.43; 124.92; 128.38; 128.93; 134.42; 137.41; 139.56; 148.99; 153.21; 160.92; 166.44; 200.50. ESI-MS HR: 464.2532 ( $M+1$ ), Calc. 464.2549.

#### 4.2.15. 4-(2,4-Diisopropylphenyl)-*N*-(3,5-dimethoxyphenyl)-4-oxo-2-(*R,S*)-(4-morpholinyl)butanamide (**15**)

$C_{28}H_{38}N_2O_5$ , starting from (*E*)-4-(2,4-diisopropylphenyl)-4-oxo-2-butenic acid (3,5-dimethoxyphenyl)amide (1.00 mmol) and a corresponding amount of morpholine, 0.235 g of **15** was obtained, 48.08% yield, orange solid, m.p. = 126–128 °C (toluene).  $^1H$  NMR (200 MHz,  $CDCl_3$ )  $\delta$ : 1.23–1.29 (overlapped *m*, 12H, *i*-Pr $CH_3$ ); 2.64 (triplet-like, 4H,  $J_{1,2}$  = 3.90 Hz, morpholino  $-CH_2-$ ); 2.88–2.98 (overlapped *m*, 2H, ABX and *i*-PrCH); 3.41–3.65 (overlapped *m*, 2H, ABX and *i*-PrCH); 3.77 (overlapped picks, 10H,  $-OCH_3$  and morpholino  $-CH_2-$ ); 4.24 (*dd*, 1H,  $J_{1,2}$  = 3.89 Hz,  $J_{1,3}$  = 7.24 Hz, ABX); 6.23 (*br*, 1H, amido-*p*-phenyl); 6.80 (*s*, 2H, amido-*o*-phenyl); 7.12 (*d*, 1H,  $J$  = 8.08, aroyl-*m*-phenyl); 7.28 (*s*, 1H, aroyl-*m*-phenyl); 7.65 (*d*, 1H,  $J$  = 7.79, aroyl-*o*-phenyl); 9.22 (*s*, 1H, amido  $-NH-$ ).  $^{13}C$  NMR (50 MHz,  $CDCl_3$ )  $\delta$ : 23.69; 24.14; 24.33; 29.11; 34.23; 36.01; 43.72; 49.98; 55.31; 64.71; 65.66; 67.31; 96.50; 97.44; 103.18; 123.23; 124.77; 128.01; 136.19; 139.38; 148.42; 152.25; 161.08; 169.67; 179.76; 194.87; 196.56; 202.57. ESI-MS HR: 483.2845 ( $M+1$ ), Calc. 483.2859.

#### 4.2.16. 4-(2,4-Diisopropylphenyl)-*N*-(3,5-dimethoxyphenyl)-4-oxo-2-(*R,S*)-[1-(4-methylpiperazinyl)butanamide (**16**)

$C_{29}H_{41}N_3O_4$ , starting from (*E*)-4-(2,4-diisopropylphenyl)-4-oxo-2-butenic acid (3,5-dimethoxyphenyl)amide (1.00 mmol) and a corresponding amount of 1-methylpiperazine, 0.298 g of **16** was obtained, 59.37% yield, orange solid, m.p. = 109–111 °C (toluene).  $^1H$  NMR (200 MHz,  $CDCl_3$ )  $\delta$ : 1.23–1.29 (overlapped *m*, 12H, *i*-Pr $CH_3$ ); 2.33 (*s*, 3H,  $-N-CH_3$ ); 2.57 (*br*, 4H, piperazine  $-CH_2-$ ); 2.67 (*br*, 4H, piperazine  $-CH_2-$ ); 2.85–2.96 (overlapped *m*, 2H, ABX and *i*-PrCH); 3.42–3.58 (overlapped *m*, 2H, ABX and *i*-PrCH); 3.78 (*s*, 6H,  $-OCH_3$ ); 4.28 (*dd*, 1H,  $J_{1,2}$  = 4.59 Hz,  $J_{1,3}$  = 8.52 Hz, ABX); 6.23 (triplet-like, 1H,  $J_{1,2}$  = 2.24 Hz, amido-*p*-phenyl); 6.79 (*s*, 1H, amido-*o*-phenyl); 6.80 (*s*, 1H, amido-*o*-phenyl); 7.11 (*d*, 1H,  $J$  = 8.11, aroyl-*m*-phenyl); 7.27 (*s*, 1H, aroyl-*m*-phenyl); 7.64 (*d*, 1H,  $J$  = 8.12, aroyl-*o*-phenyl); 9.22 (*s*, 1H, amido  $-NH-$ ).  $^{13}C$  NMR (50 MHz,  $CDCl_3$ )  $\delta$ : 23.71; 24.18; 24.31; 29.12; 34.21; 35.83; 45.85; 55.33; 55.50; 65.20; 96.32; 97.45; 123.31; 124.70; 128.03; 163.35; 139.49; 148.32; 152.10; 161.04; 169.96; 202.81. ESI-MS HR: 496.3166 ( $M+1$ ), Calc. 496.3170.

#### 4.2.17. 4-(2,4-Diisopropylphenyl)-*N*-(4-isopropylphenyl)-4-oxo-2-(*R,S*)-(1-piperidinyl)butanamide (**17**)

$C_{30}H_{42}N_2O_2$ , starting from (*E*)-4-(2,4-diisopropylphenyl)-4-oxo-2-butenic acid (4-isopropylphenyl)amide (0.79 mmol) and a corresponding amount of piperidine, 0.160 g of **17** was obtained, 43.46% yield, orange semi-solid.  $^1H$  NMR (200 MHz,  $CDCl_3$ )  $\delta$ : 1.20–1.30 (overlapped *d*, 18H, *i*-Pr $CH_3$ ); 1.47 (*br*, 2H, piperidinyl  $-CH_2-$ ); 1.63 (*br*, 4H, piperidinyl  $-CH_2-$ ); 2.56 (triplet-like picks, 4H,  $J$  = 14.06 Hz, piperidinyl  $-CH_2-$ ); 2.83–2.95 (overlapped *m*, 3H, ABX and *i*-PrCH); 3.41–3.60 (overlapped *m*, 2H, ABX and *i*-PrCH); 4.21 (*dd*, 1H,  $J_{1,2}$  = 8.96 Hz,  $J_{1,3}$  = 17.91 Hz, ABX); 7.09 (*d*, 1H,



$J = 8.95$  Hz, aroyl-*m*-phenyl); 7.17 (*d*, 2H,  $J = 7.68$  Hz, amido-*m*-phenyl); 7.27 (*s*, 1H, aroyl-*m*-phenyl); 7.46 (*d*, 2H,  $J = 8.96$  Hz, amido-*o*-phenyl); 7.66 (*d*, 1H,  $J = 8.96$  Hz, aroyl-*o*-phenyl); 9.32 (*s*, 1H, amido-NH-);  $^{13}\text{C}$  NMR (50 MHz,  $\text{CDCl}_3$ )  $\delta$ : 23.71; 23.96; 24.18; 24.36; 26.69; 29.13; 33.52; 34.21; 36.13; 51.07; 66.06; 119.35; 123.19; 124.63; 126.80; 128.11; 135.61; 144.58; 148.26; 151.94; 170.35; 203.30. ESI-MS HR: 463.3322 ( $M+1$ ), Calc. 463.3319.

#### 4.2.18. 4-(2,4-Diisopropylphenyl)-*N*-(4-isopropylphenyl)-4-oxo-2-(*R,S*)-(1-imidazolyl)butanamide (**18**)

$\text{C}_{28}\text{H}_{35}\text{N}_3\text{O}_2$ , starting from (*E*)-4-(2,4-diisopropylphenyl)-4-oxo-2-butenic acid (4-isopropylphenyl)amide (0.79 mmol) and a corresponding amount of imidazole, **18** was obtained, in quantitative yield, orange semi-solid.  $^1\text{H}$  NMR (200 MHz,  $\text{CDCl}_3$ )  $\delta$ : 1.12–1.25 (overlapped *d*, 18H, *i*-PrCH<sub>3</sub>); 2.83–2.92 (overlapped *m*, 2H, *i*-PrCH); 3.36 (triplet-like, 1H,  $J_{1,2} = 6.71$  Hz, *i*-PrCH); 3.46 (*dd*, 1H,  $J_{1,2} = 5.25$  Hz,  $J_{1,3} = 17.44$  Hz, ABX); 4.00 (*dd*, 1H,  $J_{1,2} = 6.15$  Hz,  $J_{1,3} = 17.89$  Hz, ABX); 5.69 (*br*, 1H, ABX); 7.08 (*d*, 1H,  $J = 7.71$  Hz, aroyl-*m*-phenyl); 7.12 (*d*, 2H,  $J = 8.05$  Hz, amido-*m*-phenyl); 7.17 (*s*, 1H, imidazolyl-CH-); 7.24 (*s br*, 1H, imidazolyl-CH-); 7.26 (*s*, 1H, aroyl-*m*-phenyl); 7.44 (*d*, 2H,  $J = 7.49$  Hz, amido-*o*-phenyl); 7.48 (*d*, 1H,  $J = 8.05$  Hz, aroyl-*o*-phenyl); 7.77 (*s*, 1H, imidazolyl-CH-); 9.32 (*s*, 1H, amido-NH-);  $^{13}\text{C}$  NMR (125 MHz,  $\text{CDCl}_3$ )  $\delta$ : 23.68; 23.95; 24.07; 29.08; 33.58; 34.31; 45.12; 57.18; 117.93; 120.26; 123.51; 124.93; 126.81; 128.31; 134.48; 135.17; 145.53; 148.96; 153.18; 166.18; 200.44. ESI-MS HR: 446.2806 ( $M+1$ ), Calc. 446.2808.

#### 4.2.19. 4-(2,4-Diisopropylphenyl)-*N*-(4-isopropylphenyl)-4-oxo-2-(*R,S*)-(4-morpholinyl)butanamide (**19**)

$\text{C}_{29}\text{H}_{40}\text{N}_2\text{O}_3$ , starting from (*E*)-4-(2,4-diisopropylphenyl)-4-oxo-2-butenic acid (4-isopropylphenyl)amide (0.79 mmol) and a corresponding amount of morpholine, **19** was obtained, in quantitative yield, orange semi-solid.  $^1\text{H}$  NMR (200 MHz,  $\text{CDCl}_3$ )  $\delta$ : 1.23–1.30 (overlapped *d*, 18H, *i*-PrCH<sub>3</sub>); 2.64 (triplet-like picks, 4H, morpholino-CH<sub>2</sub>-); 2.84–2.97 (overlapped *m*, 3H, ABX and *i*-PrCH); 3.40–3.64 (overlapped *m*, 2H, *i*-PrCH and ABX); 3.77 (*br*, 4H, morpholino-CH<sub>2</sub>-); 4.24 (*dd*, 1H,  $J_{1,2} = 4.43$  Hz,  $J_{1,3} = 8.07$  Hz, ABX); 7.09–7.13 (doublet-like signal, 1H, aroyl-*m*-phenyl); 7.18 (*d*, 2H,  $J = 8.41$  Hz,  $J = 8.41$  Hz, amido-*m*-phenyl); 7.28 (*s*, 1H, aroyl-*m*-phenyl); 7.46 (*d*, 2H,  $J = 8.41$  Hz, amido-*o*-phenyl); 7.65 (*d*, 1H,  $J = 7.84$  Hz, aroyl-*o*-phenyl); 9.16 (*s*, 1H, amido-NH-);  $^{13}\text{C}$  NMR (50 MHz,  $\text{CDCl}_3$ )  $\delta$ : 23.69; 23.94; 24.18; 24.29; 29.15; 33.50; 34.21; 36.20; 50.02; 65.44; 67.31; 119.42; 123.25; 124.70; 126.85; 128.13; 128.98; 135.30; 136.21; 144.89; 148.35; 152.19; 169.45; 202.72. ESI-MS HR: 465.3114 ( $M+1$ ), Calc. 465.3117.

#### 4.2.20. 4-(2,4-Diisopropylphenyl)-*N*-(4-isopropylphenyl)-4-oxo-2-(*R,S*)-[1-(4-methyl-piperazinyl)]butanamide (**20**)

$\text{C}_{30}\text{H}_{43}\text{N}_3\text{O}_2$ , starting from (*E*)-4-(2,4-diisopropylphenyl)-4-oxo-2-butenic acid (4-isopropylphenyl)amide (0.79 mmol) and a corresponding amount of 1-methylpiperazine, **20** was obtained, in quantitative yield, orange semi-solid.  $^1\text{H}$  NMR (200 MHz,  $\text{CDCl}_3$ )  $\delta$ : 1.21–1.29 (overlapped *d*, 18H, *i*-PrCH<sub>3</sub>); 2.32 (*s*, 3H, N-CH<sub>3</sub>); 2.53 (*br*, 4H, piperazine-CH<sub>2</sub>-); 2.67 (*br*, 4H, piperazine-CH<sub>2</sub>-); 2.80–2.97 (overlapped *m*, 3H, ABX and *i*-PrCH); 3.38–3.61 (overlapped *m*, 2H, ABX and *i*-PrCH); 4.28 (*dd*, 1H,  $J_{1,2} = 4.53$  Hz,  $J_{1,3} = 7.76$  Hz, ABX); 7.07–7.12 (doublet-like signals, 1H, aroyl-*m*-phenyl); 7.17 (*d*, 2H,  $J = 8.57$  Hz, amido-*m*-phenyl); 7.26 (*s*, 1H, aroyl-*m*-phenyl); 7.46 (*d*, 2H,  $J = 8.57$  Hz, amido-*o*-phenyl); 7.63 (*d*, 1H,  $J = 8.20$  Hz, aroyl-*o*-phenyl); 9.16 (*s*, 1H, amido-NH-);  $^{13}\text{C}$  NMR (50 MHz,  $\text{CDCl}_3$ )  $\delta$ : 23.71; 23.96; 24.22; 24.29; 29.17; 33.50; 34.21; 36.00; 45.88; 55.52; 65.02; 119.39; 123.25; 124.63; 126.83; 128.18; 135.43; 136.39; 144.75; 148.24; 152.05; 169.75; 202.97. ESI-MS HR: 478.3429 ( $M+1$ ), Calc. 478.3428.

#### 4.2.21. *N*-cyclohexyl-4-(2,4-diisopropylphenyl)-4-oxo-2-(*R,S*)-(1-piperidinyl)butanamide (**21**)

$\text{C}_{27}\text{H}_{42}\text{N}_2\text{O}_2$ , starting from (*E*)-4-(2,4-diisopropylphenyl)-4-oxo-2-butenic acid cyclohexylamide (0.88 mmol) and a corresponding amount of piperidine, 0.151 g of **21** was obtained, 40.22% yield, white solid, m.p. = 105–107 °C (toluene).  $^1\text{H}$  NMR (200 MHz,  $\text{CDCl}_3$ )  $\delta$ : 1.09–1.46 (overlapped *m*, 8H, cyclohexyl-CH<sub>2</sub>- and piperidinyl-CH<sub>2</sub>-); 1.22–1.28 (overlapped *d*, 12H, *i*-PrCH<sub>3</sub>); 1.54–1.70 (overlapped *m*, 6H, piperidinyl-CH<sub>2</sub>- and cyclohexyl-CH<sub>2</sub>-); 1.84 (*br*, 2H, cyclohexyl-CH<sub>2</sub>-); 2.47 (triplet-like, 4H,  $J = 6.97$  Hz, piperidinyl-CH<sub>2</sub>-); 2.97 (*dd*, 1H,  $J_{1,2} = 4.65$  Hz,  $J_{1,3} = 16.27$  Hz, ABX); 2.91 (*m*, 1H, *i*-PrCH); 3.35–3.53 (overlapped *m*, 2H, ABX and *i*-PrCH); 3.74 (*m*, 1H, cyclohexyl-CH-); 4.03 (*dd*, 1H,  $J_{1,2} = 4.59$  Hz,  $J_{1,3} = 17.91$  Hz, ABX); 7.09 (*d*, 1H,  $J = 7.83$  Hz, aroyl-*m*-phenyl); 7.24 (*s*, 1H, aroyl-*m*-phenyl); 7.66 (*d*, 1H,  $J = 7.83$  Hz, aroyl-*o*-phenyl); 6.75 (*d*, 1H,  $J = 13.78$  Hz, amido-NH-).  $^{13}\text{C}$  NMR (50 MHz,  $\text{CDCl}_3$ )  $\delta$ : 22.31; 22.43; 23.71; 24.00; 24.18; 24.31; 24.58; 25.47; 26.53; 29.12; 32.88; 33.14; 34.18; 36.36; 44.43; 47.41; 50.89; 65.33; 95.73; 123.17; 124.47; 128.14; 136.70; 170.96; 203.83. ESI-MS HR: 427.3323 ( $M+1$ ), Calc. 427.3325.

#### 4.2.22. *N*-cyclohexyl-4-(2,4-diisopropylphenyl)-4-oxo-2-(*R,S*)-(1-imidazolyl)butanamide (**22**)

$\text{C}_{25}\text{H}_{35}\text{N}_3\text{O}_2$ , starting from (*E*)-4-(2,4-diisopropylphenyl)-4-oxo-2-butenic acid cyclohexylamide (0.88 mmol) and a corresponding amount of imidazole, 0.170 g of **22** was obtained, 47.17% yield, white solid, m.p. = 123–125 °C (toluene).  $^1\text{H}$  NMR (200 MHz,  $\text{CDCl}_3$ )  $\delta$ : 1.04–1.35 (overlapped *m*, 6H, cyclohexyl-CH<sub>2</sub>-); 1.12–1.26 (overlapped *d*, 12H, *i*-PrCH<sub>3</sub>); 1.53–1.69 (*br*, 2H, cyclohexyl-CH<sub>2</sub>-); 1.83 (*br*, 2H, cyclohexyl-CH<sub>2</sub>-); 2.91 (*m*, 1H,  $J_{1,2} = 6.67$  Hz,  $J_{1,3} = 13.34$  Hz, *i*-PrCH); 3.25–3.45 (overlapped *m*, 2H, ABX and *i*-PrCH); 3.73 (*m*, 1H, cyclohexyl-CH-); 3.96 (*dd*, 1H,  $J_{1,2} = 6.19$  Hz,  $J_{1,3} = 17.98$  Hz, ABX); 5.40 (*t*, 1H,  $J_{1,2} = 6.67$  Hz, ABX); 6.32 (*s br*, 1H, amido-NH-); 7.06–7.11 (overlapped *m*, 2H, aroyl-*m*-phenyl and imidazolyl-CH-); 7.24 (doublet-like, 1H, aroyl-*m*-phenyl); 7.46 (*d*, 1H,  $J = 7.81$  Hz, aroyl-*o*-phenyl); 7.57 (*s*, 1H, imidazolyl-CH-);  $^{13}\text{C}$  NMR (50 MHz,  $\text{CDCl}_3$ )  $\delta$ : 26.62; 23.94; 24.04; 24.62; 25.24; 29.01; 32.48; 34.23; 45.19; 48.80; 56.64; 95.73; 117.73; 123.39; 124.85; 128.13; 130.09; 134.70; 137.43; 148.72; 153.01; 167.34; 200.70. ESI-MS HR: 410.2813 ( $M+1$ ), Calc. 410.2802.

#### 4.2.23. *N*-cyclohexyl-4-(2,4-diisopropylphenyl)-4-oxo-2-(*R,S*)-(4-morpholinyl)butanamide (**23**)

$\text{C}_{26}\text{H}_{40}\text{N}_2\text{O}_3$ , starting from (*E*)-4-(2,4-diisopropylphenyl)-4-oxo-2-butenic acid cyclohexylamide (1.00 mmol) and a corresponding amount of morpholine, 0.372 g of **23** was obtained, 84.55% yield, white solid, m.p. = 142–144 °C (toluene).  $^1\text{H}$  NMR (200 MHz,  $\text{CDCl}_3$ )  $\delta$ : 1.11–1.41 (*br*, 6H, cyclohexyl-CH<sub>2</sub>-); 1.23–1.29 (overlapped *d*, 12H, *i*-PrCH<sub>3</sub>); 1.65 (*br*, 2H, cyclohexyl-CH<sub>2</sub>-); 1.86 (*br*, 2H, cyclohexyl-CH<sub>2</sub>-); 2.56 (triplet-like, 4H,  $J_{1,2} = 4.40$  Hz, morpholino-CH<sub>2</sub>-); 2.78–2.95 (overlapped *m*, 2H, ABX and *i*-PrCH); 3.35–3.58 (overlapped *m*, 2H, ABX and *i*-PrCH); 3.72 (quartet-like, 4H,  $J_{1,2} = 3.64$  Hz,  $J_{1,3} = 8.80$  Hz, morpholino-CH<sub>2</sub>-); 3.79 (*m*, 1H, cyclohexyl-CH-); 4.05 (*dd*, 1H,  $J_{1,2} = 4.43$  Hz,  $J_{1,3} = 8.07$  Hz, ABX); 7.07–7.12 (overlapped *m*, aroyl-*m*-phenyl and amido-NH-); 7.24 (*br*, 1H, aroyl-*m*-phenyl); 7.64 (*d*, 1H,  $J = 7.81$  Hz, aroyl-*o*-phenyl);  $^{13}\text{C}$  NMR (50 MHz,  $\text{CDCl}_3$ )  $\delta$ : 23.71; 24.22; 24.29; 24.64; 25.46; 29.19; 32.92; 33.25; 34.21; 36.62; 47.67; 49.96; 64.78; 67.26; 123.26; 124.57; 128.18; 136.41; 148.12; 152.03; 170.09; 203.21. ESI-MS HR: 429.3123 ( $M+1$ ), Calc. 429.3112.

#### 4.2.24. *N*-cyclohexyl-4-(2,4-diisopropylphenyl)-4-oxo-2-(*R,S*)-[1-(4-methylpiperazinyl)]butanamide (**24**)

$\text{C}_{27}\text{H}_{43}\text{N}_3\text{O}_2$ , starting from (*E*)-4-(2,4-diisopropylphenyl)-4-oxo-2-butenic acid cyclohexylamide (1.00 mmol) and a corresponding

amount of 1-methylpiperazine, 0.256 g of **24** was obtained, 56.47% yield, white solid, m.p. = 96–98 °C (toluene). <sup>1</sup>H NMR (200 MHz, CDCl<sub>3</sub>) δ: 1.15–1.39 (br, 6H, cyclohexyl –CH<sub>2</sub>–); 1.22–1.27 (overlapped d, 12H, *i*-PrCH<sub>3</sub>); 1.65 (br, 2H, cyclohexyl –CH<sub>2</sub>–); 1.86 (br, 2H, cyclohexyl –CH–); 2.33 (s, 3H, piperazine-*N*-CH<sub>3</sub>); 2.52 (br, 4H, piperazine –CH<sub>2</sub>–); 2.60 (br, 4H, piperazine –CH<sub>2</sub>–); 2.76–2.96 (overlapped m, 2H, ABX and *i*-PrCH); 3.34–3.55 (overlapped m, 2H, ABX and *i*-PrCH); 3.76 (m, 1H, cyclohexyl –CH–); 4.10 (dd, 1H, *J*<sub>1,2</sub> = 4.50 Hz, *J*<sub>1,3</sub> = 9.00 Hz, ABX); 7.04–7.11 (overlapped m, aroyl-*m*-phenyl and cyclohexyl-NH); 7.24 (s, 1H, aroyl-*m*-phenyl); 7.64 (d, 1H, *J* = 8.04, aroyl-*o*-phenyl); <sup>13</sup>C NMR (50 MHz, CDCl<sub>3</sub>) δ: 23.67; 24.18; 24.58; 25.42; 29.15; 32.87; 33.18; 34.16; 36.36; 45.68; 47.56; 55.32; 64.31; 123.31; 124.43; 128.14; 136.54; 147.91; 151.81; 170.26; 203.41. ESI-MS HR: 442.3436 (M+1), Calc. 442.3428.

4.2.25. *N*-(3,5-dimethoxyphenyl)-4-oxo-2-(*R,S*)-(1-piperidinyl)-4-(5,6,7,8-tetrahydronaphthalenyl)butanamide (**25**)

C<sub>27</sub>H<sub>43</sub>N<sub>3</sub>O<sub>2</sub>, starting from (*E*)-4-oxo-4-(5,6,7,8-tetrahydronaphthalenyl)-2-butenic acid (3,5-dimethoxyphenyl)-amide (0.82 mmol) and a corresponding amount of piperidine, 0.239 g of **25** was obtained, 64.61% yield, pale yellow solid, m.p. = 135 °C (toluene). <sup>1</sup>H NMR (200 MHz, CDCl<sub>3</sub>) δ: 1.48 (quartet-like signals, 2H, piperidinyl –CH<sub>2</sub>–); 1.65 (quartet-like signals, 4H, piperidinyl –CH<sub>2</sub>–); 1.81 (br, 4H, tetralinoyl –CH<sub>2</sub>–); 2.57 (triplet-like signals, 4H, piperidinyl –CH–); 2.82 (br, 4H, tetralinoyl –CH<sub>2</sub>–); 3.00 (dd, 1H, *J*<sub>1,2</sub> = 5.06, *J*<sub>1,3</sub> = 16.85, ABX); 3.68 (dd, 1H, *J*<sub>1,2</sub> = 7.30, *J*<sub>1,3</sub> = 17.41, ABX); 3.77 (s, 6H, –OCH<sub>3</sub>); 4.25 (dd, 1H, *J*<sub>1,2</sub> = 5.06, *J*<sub>1,3</sub> = 6.74, ABX); 6.22 (triplet-like signals, 1H, amido-*p*-phenyl); 6.79 (s, 1H, amido-*o*-phenyl); 6.80 (s, 1H, amido-*o*-phenyl); 7.15 (d, 1H, *J* = 8.99, aroyl-*m*-phenyl); 7.73 (m, 2H, aroyl-*o*-phenyl); 7.74 (m, 2H, aroyl-*o*-phenyl); 9.48 (s, 1H, amide –NH–). <sup>13</sup>C NMR (50 MHz, CDCl<sub>3</sub>) δ: 22.34; 22.54; 22.76; 22.89; 23.89; 26.73; 29.32; 29.55; 31.92; 44.50; 51.04; 55.33; 65.57; 96.34; 97.37; 125.30; 129.14; 129.31; 134.42; 137.39; 139.65; 143.16; 161.06; 170.71; 198.40. ESI-MS HR: 451.2594 (M+1), Calc. 451.2591.

4.2.26. *N*-(3,5-dimethoxyphenyl)-4-oxo-2-(*R,S*)-(1-imidazolyl)-4-(5,6,7,8-tetrahydronaphthalenyl)butanamide (**26**)

C<sub>25</sub>H<sub>27</sub>N<sub>3</sub>O<sub>4</sub>, starting from (*E*)-4-oxo-4-(5,6,7,8-tetrahydronaphthalenyl)-2-butenic acid (3,5-dimethoxyphenyl)-amide (0.82 mmol) and a corresponding amount of imidazole, 0.279 g of **26** was obtained, 78.49% yield, white solid, m.p. = 166 °C. <sup>1</sup>H NMR (200 MHz, CDCl<sub>3</sub>) δ: 1.80 (br, 4H, tetralinoyl –CH<sub>2</sub>–); 2.78 (br, 4H, tetralinoyl –CH<sub>2</sub>–); 3.48 (dd, 1H, *J*<sub>1,2</sub> = 5.33, *J*<sub>1,3</sub> = 17.69, ABX); 3.73 (s, 6H, –OCH<sub>3</sub>); 4.07 (dd, 1H, *J*<sub>1,2</sub> = 7.58, *J*<sub>1,3</sub> = 17.41, ABX); 5.58 (t-like signals, 1H, ABX); 6.17 (sb, 1H, amido-*p*-phenyl); 6.76 (sb, 2H, amido-*o*-phenyl); 6.98 (s, 1H, imidazolyl –CH–); 7.07 (d, 1H, *J* = 8.43 Hz, aroyl-*m*-phenyl); 7.17 (s, 1H, imidazolyl –CH–); 7.58 (br, 2H, aroyl-*o*-phenyl); 7.77 (s, 1H, imidazolyl –CH–); 9.99 (s, 1H, amide –NH–). <sup>13</sup>C NMR (50 MHz, CDCl<sub>3</sub>) δ: 22.47; 22.62; 29.08; 29.46; 41.41; 55.10; 56.63; 96.95; 98.05; 117.87; 124.98; 128.80; 128.94; 129.40; 133.06; 136.94; 137.59; 139.40; 144.27; 160.75; 196.22. ESI-MS HR: 434.2084 (M+1), Calc. 434.2074.

4.2.27. *N*-(3,5-dimethoxyphenyl)-4-oxo-2-(*R,S*)-(4-morpholinyl)-4-(5,6,7,8-tetrahydronaphthalenyl)butanamide (**27**)

C<sub>26</sub>H<sub>32</sub>N<sub>2</sub>O<sub>5</sub>, starting from (*E*)-4-oxo-4-(5,6,7,8-tetrahydronaphthalenyl)-2-butenic acid (3,5-dimethoxyphenyl)-amide (1.00 mmol) and a corresponding amount of morpholine, 0.261 g of **27** was obtained, 52.69% yield, white solid, m.p. = 179–181 °C (toluene). <sup>1</sup>H NMR (200 MHz, CDCl<sub>3</sub>) δ: 1.81 (br, 4H, tetralinoyl –CH<sub>2</sub>–); 2.65 (triplet-like, 4H, *J*<sub>1,2</sub> = 4.41 Hz, morpholino –CH<sub>2</sub>–); 2.81 (br, 4H, tetralinoyl –CH<sub>2</sub>–); 3.04 (dd, 1H, *J*<sub>1,2</sub> = 4.99 Hz, *J*<sub>1,3</sub> = 16.75 Hz, ABX); 3.64–3.89 (overlapped signals, 11H, ABX, –OCH<sub>3</sub> and morpholino –CH<sub>2</sub>–); 4.24 (triplet-like, 1H, *J*<sub>1,2</sub> = 5.06 Hz,

ABX); 6.23 (t-like, 1H, *J*<sub>1,2</sub> = 2.29 Hz, amido-*p*-phenyl); 6.78 (s, 1H, amido-*o*-phenyl); 6.79 (s, 1H, amido-*o*-phenyl); 7.15 (d, 1H, *J* = 9.00 Hz, aroyl-*m*-phenyl); 7.72 (br, 2H, aroyl-*o*-phenyl); 9.22 (s, 1H, amide –NH–). <sup>13</sup>C NMR (50 MHz, CDCl<sub>3</sub>) δ: 22.73; 22.87; 29.32; 29.57; 32.16; 50.02; 55.35; 66.02; 67.35; 95.73; 96.48; 97.46; 125.27; 129.14; 129.38; 134.21; 137.48; 139.40; 143.42; 161.08; 169.82; 197.86. ESI-MS HR: 453.2387 (M+1), Calc. 453.2389.

4.2.28. *N*-(3,5-dimethoxyphenyl)-4-oxo-2-(*R,S*)-[1-(4-methylpiperazinyl)]-4-(5,6,7,8-tetrahydronaphthalenyl)butanamide (**28**)

C<sub>27</sub>H<sub>35</sub>N<sub>3</sub>O<sub>4</sub>, starting from (*E*)-4-oxo-4-(5,6,7,8-tetrahydronaphthalenyl)-2-butenic acid (3,5-dimethoxyphenyl)-amide (0.82 mmol) and a corresponding amount of 1-methylpiperazine, 0.247 g of **28** was obtained, 64.42% yield, pale yellow solid, m.p. = 106–108 °C (toluene). <sup>1</sup>H NMR (200 MHz, CDCl<sub>3</sub>) δ: 1.81 (br, 4H, tetralinoyl –CH<sub>2</sub>–); 2.34 (s, 3H, piperazine-*N*-CH<sub>3</sub>); 2.55 (br, 4H, piperazine –CH<sub>2</sub>–); 2.69 (br, 4H, piperazine –CH<sub>2</sub>–); 2.81 (br, 4H, tetralinoyl –CH<sub>2</sub>–); 3.03 (dd, 1H, *J*<sub>1,2</sub> = 4.96 Hz, *J*<sub>1,3</sub> = 17.37 Hz, ABX); 3.67 (dd, 1H, *J*<sub>1,2</sub> = 7.14 Hz, *J*<sub>1,3</sub> = 17.37 Hz, ABX); 3.77 (s, 6H, –OCH<sub>3</sub>); 4.31 (dd, 1H, *J*<sub>1,2</sub> = 4.96 Hz, *J*<sub>1,3</sub> = 9.31 Hz, ABX); 6.23 (br, 1H, amido-*p*-phenyl); 6.79 (s, 1H, amido-*o*-phenyl); 6.80 (s, 1H, amido-*o*-phenyl); 7.14 (d, 1H, *J* = 8.57 Hz, aroyl-*m*-phenyl); 7.71–7.73 (overlapped signals, 2H, aroyl-*o*-phenyl); 9.29 (s, 1H, amide –NH–). <sup>13</sup>C NMR (50 MHz, CDCl<sub>3</sub>) δ: 22.73; 22.87; 29.30; 29.55; 31.86; 45.76; 55.35; 55.50; 64.51; 96.30; 97.50; 125.25; 129.14; 129.33; 134.30; 137.41; 139.52; 143.31; 161.06; 170.07; 198.04. ESI-MS HR: 466.2707 (M+1), Calc. 466.2706.

4.2.29. *N*-(4-isopropylphenyl)-4-oxo-2-(*R,S*)-(1-piperidinyl)-4-(5,6,7,8-tetrahydronaphthalenyl)butanamide (**29**)

C<sub>28</sub>H<sub>36</sub>N<sub>2</sub>O<sub>2</sub>, starting from (*E*)-4-oxo-4-(5,6,7,8-tetrahydronaphthalenyl)-2-butenic acid (4-isopropylphenyl)-amide (0.86 mmol) and a corresponding amount of piperidine, 0.373 g of **29** was obtained, in quantitative yield, as yellow semi-solid. <sup>1</sup>H NMR (200 MHz, CDCl<sub>3</sub>) δ: 1.22 (d, 6H, *J* = 7.09, 4-*i*-PrCH<sub>3</sub>); 1.47 (q, 2H, *J*<sub>1,2</sub> = 5.38, *J*<sub>1,3</sub> = 10.75, piperidine –CH<sub>2</sub>–); 1.64 (q, 4H, *J*<sub>1,2</sub> = 5.37, *J*<sub>1,3</sub> = 10.75, piperidine –CH<sub>2</sub>–); 1.80 (br, 4H, tetralinoyl –CH<sub>2</sub>–); 2.57 (t, 4H, *J*<sub>1,2</sub> = 5.07, piperidine –CH<sub>2</sub>–); 2.80 (br, 5H, tetralinoyl –CH<sub>2</sub>– and 4-*i*-Pr-CH); 2.96 (dd, 1H, *J*<sub>1,2</sub> = 5.02, *J*<sub>1,3</sub> = 19.07, ABX); 3.68 (dd, 1H, *J*<sub>1,2</sub> = 6.91, *J*<sub>1,3</sub> = 16.57, ABX); 4.25 (t, 1H, *J*<sub>1,2</sub> = 5.56, ABX); 7.14 (d, 1H, *J* = 8.51, aroyl-*m*-phenyl); 7.16 (d, 2H, *J* = 8.06, amido-*m*-phenyl); 7.46 (d, 1H, *J* = 8.51, amido-*o*-phenyl); 7.73 (s, 1H, aroyl-*o*-phenyl); 7.76 (s, 1H, aroyl-*o*-phenyl); 9.40 (s, 1H, amide –NH–). <sup>13</sup>C NMR (50 MHz, CDCl<sub>3</sub>) δ: 22.76; 22.89; 23.94; 26.69; 29.30; 29.53; 31.96; 33.49; 51.04; 65.71; 95.70; 119.29; 125.30; 126.76; 129.13; 134.53; 135.57; 137.34; 143.02; 144.53; 170.44; 198.59. ESI-MS HR: 433.2868 (M+1), Calc. 433.2849.

4.2.30. *N*-(4-isopropylphenyl)-4-oxo-2-(*R,S*)-(1-imidazolyl)-4-(5,6,7,8-tetrahydronaphthalenyl)butanamide (**30**)

C<sub>26</sub>H<sub>29</sub>N<sub>3</sub>O<sub>2</sub>, starting from (*E*)-4-oxo-4-(5,6,7,8-tetrahydronaphthalenyl)-2-butenic acid (4-isopropylphenyl)-amide (0.86 mmol) and a corresponding amount of imidazole, 0.100 g of **30** was obtained, 28.00% yield, as yellow solid, m.p. 92 °C. <sup>1</sup>H NMR (200 MHz, CDCl<sub>3</sub>) δ: 1.17 (d, 6H, *J*<sub>1,2</sub> = 7.31, *i*-PrCH<sub>3</sub>); 1.78 (br, 4H, tetralinoyl –CH<sub>2</sub>–); 2.75–2.78 (5H, overlapped signals, 4-*i*-Pr-CH– and tetralinoyl –CH<sub>2</sub>–); 3.48 (dd, 1H, *J*<sub>1,2</sub> = 5.61, *J*<sub>1,3</sub> = 17.97, ABX); 4.08 (dd, 1H, *J*<sub>1,2</sub> = 7.30, *J*<sub>1,3</sub> = 17.41, ABX); 5.64 (dd, 1H, *J*<sub>1,2</sub> = 5.61, *J*<sub>1,3</sub> = 7.30, ABX); 7.08 (d, 2H, *J* = 8.43, amido-*m*-phenyl); 7.13 (br, 2H, imidazolyl –CH–); 7.20 (s, 1H, aroyl-*m*-phenyl); 7.44 (d, 2H, *J* = 8.42, amido-*o*-phenyl); 7.60 (br, 1H, imidazolyl –CH–); 7.62 (br, 2H, aroyl-*o*-phenyl); 9.95 (s, 1H, amide –NH–). <sup>13</sup>C NMR (50 MHz, CDCl<sub>3</sub>) δ: 22.615; 22.761; 23.908; 29.224; 29.588; 33.503;

41.751; 56.699; 118.057; 120.169; 125.122; 126.761; 129.091; 129.492; 133.279; 135.500; 137.394; 137.648; 144.185; 145.277; 166.452; 196.130. ESI-MS HR: 416.2342 (M+1), Calc. 416.2333.

**4.2.31. *N*-(4-isopropylphenyl)-4-oxo-2-(*R,S*)-(4-morpholinyl)-4-(5,6,7,8-tetrahydronaphthalenyl)butanamide (**31**)**

C<sub>27</sub>H<sub>34</sub>N<sub>2</sub>O<sub>3</sub>, starting from (*E*)-4-oxo-4-(5,6,7,8-tetrahydronaphthalenyl)-2-butenic acid (4-isopropylphenyl) amide (0.86 mmol) and a corresponding amount of morpholine, 0.365 g of **31** was obtained, 97.28% yield, as white solid, m.p. 129–131 °C (toluene). <sup>1</sup>H NMR (200 MHz, CDCl<sub>3</sub>) δ: 1.22 (*d*, 6H, *J* = 6.52 Hz, *i*-PrCH<sub>3</sub>); 1.81 (*br*, 4H, tetralinoyl –CH<sub>2</sub>–); 2.65 (triplet-like, 4H, *J*<sub>1,2</sub> = 4.53 Hz, morpholino –CH<sub>2</sub>–); 2.81 (*br*, 5H, tetralinoyl –CH<sub>2</sub>– and *i*-PrCH); 3.33 (*dd*, 1H, *J*<sub>1,2</sub> = 5.00 Hz, *J*<sub>1,3</sub> = 16.92 Hz, ABX); 3.65–3.77 (overlapped *m*, 5H, morpholino –CH<sub>2</sub>– and ABX); 4.27 (*dd*, 1H, *J*<sub>1,2</sub> = 5.72 Hz, *J*<sub>1,3</sub> = 9.05 Hz, ABX); 7.12–7.19 (overlapped *d*, 3H, amido-*m*-phenyl and aroyl-*m*-phenyl); 7.42 (*d*, 2H, *J* = 8.61 Hz, amido-*o*-phenyl); 7.72 (*br*, 2H, aroyl-*o*-phenyl); 9.17 (*s*, 1H, amido –NH–). <sup>13</sup>C NMR (50 MHz, CDCl<sub>3</sub>) δ: 22.73; 22.85; 23.93; 29.28; 29.53; 32.21; 33.49; 50.04; 65.09; 67.33; 119.39; 125.25; 126.81; 129.34; 134.30; 135.30; 137.43; 143.31; 144.86; 169.56; 198.02. ESI-MS HR: 435.2654 (M+1), Calc. 435.2648.

**4.2.32. *N*-(4-isopropylphenyl)-4-oxo-2-(*R,S*)-[1-(4-methylpiperazinyl)]-4-(5,6,7,8-tetrahydronaphthalenyl)butanamide (**32**)**

C<sub>28</sub>H<sub>37</sub>N<sub>3</sub>O<sub>2</sub>, starting from (*E*)-4-oxo-4-(5,6,7,8-tetrahydronaphthalenyl)-2-butenic acid (4-isopropylphenyl) amide (1.15 mmol) and a corresponding amount of 1-methylpiperazine, 0.432 g of **32** was obtained, 83.83% yield, as orange semi-solid. <sup>1</sup>H NMR (200 MHz, CDCl<sub>3</sub>) δ: 1.22 (*d*, 6H, *J* = 6.60, *i*-PrCH<sub>3</sub>); 1.81(*br*, 4H, tetralinoyl –CH<sub>2</sub>–); 2.32 (*s*, 3H, piperazine-*N*-CH<sub>3</sub>); 2.52 (*br*, 4H, piperazine –CH<sub>2</sub>–); 2.68 (*br*, 4H, piperazine –CH<sub>2</sub>–); 2.80 (*br*, 4H, tetralinoyl –CH<sub>2</sub>–); 2.96 (triplet-like, 1H, *J*<sub>1,2</sub> = 2.73, ABX); 2.96 (*m*, 1H, *i*-PrCH); 3.68 (*dd*, 1H, *J*<sub>1,2</sub> = 7.16 Hz, *J*<sub>1,3</sub> = 16.93 Hz, ABX); 4.33 (*dd*, 1H, *J*<sub>1,2</sub> = 5.16 Hz, *J*<sub>1,3</sub> = 7.04, ABX); 7.13 (*d*, 1H, *J* = 8.11, aroyl-*m*-phenyl); 7.17 (*d*, 2H, *J* = 8.52, amido-*m*-phenyl); 7.46 (*d*, 2H, *J* = 8.52, amido-*o*-phenyl); 7.72 (*s*, 1H, aroyl-*o*-phenyl); 7.73 (*d*, 1H, *J* = 5.41, aroyl-*o*-phenyl); 9.24 (*s*, 1H, amido –NH–). <sup>13</sup>C NMR (50 MHz, CDCl<sub>3</sub>) δ: 22.76; 22.91; 23.98; 29.31; 29.57; 31.88; 33.52; 44.30; 45.92; 55.59; 64.67; 119.37; 125.28; 126.83; 129.16; 129.33; 134.44; 135.44; 137.39; 143.20; 144.75; 168.89; 198.27. ESI-MS HR: 448.2966 (M+1), Calc. 448.2964.

**4.2.33. *N*-cyclohexyl-4-oxo-2-(*R,S*)-1-piperidinyl-4-(5,6,7,8-tetrahydronaphthalenyl)butanamide (**33**)**

C<sub>25</sub>H<sub>36</sub>N<sub>2</sub>O<sub>2</sub>, starting from (*E*)-4-oxo-4-(5,6,7,8-tetrahydronaphthalenyl)-2-butenic acid cyclohexylamide (0.96 mmol) and a corresponding amount of piperidine, 0.200 g of **33** was obtained, 52.35% yield, as pale yellow solid, m.p. 78 °C (toluene). <sup>1</sup>H NMR (500 MHz, CDCl<sub>3</sub>) δ: 1.19 (*m*, 2H, ax C2, cyclohexyl –CH–); 1.36 (*m*, 2H, ax C3, cyclohexyl –CH–); 1.44 (*m*, 1H, ax C4, cyclohexyl –CH–); 1.55 (*m*, 4H, C3, piperidine –CH<sub>2</sub>–); 1.60 (*m*, 1H, eq C4, cyclohexyl –CH–); 1.62 (*m*, 2H, C4, piperidine –CH<sub>2</sub>–); 1.68 (*m*, 2H, eq C3, cyclohexyl –CH–); 1.80 (doublet-like signal, 4H, β-tetralinyl); 1.86 (*m*, 2H, eq C2, cyclohexyl –CH–); 2.49 and 2.54 (*m*, *br*, 4H, piperidine –CH–); 2.80 (doublet-like signal, 4H, β-tetralinyl); 2.87 (*dd*, 1H, *J*<sub>1,2</sub> = 5.31, *J*<sub>1,3</sub> = 16.26, ABX); 3.60 (*dd*, 1H, *J*<sub>1,2</sub> = 7.19, *J*<sub>1,3</sub> = 16.26, ABX); 3.75 (doublet-like signal, 1H, cyclohexyl –CH–); 4.06 (*dd*, 1H, *J*<sub>1,2</sub> = 5.32, *J*<sub>1,3</sub> = 7.04, ABX); 7.13 (*d*, 1H, *J* = 8.29, aroyl-*m*-phenyl); 7.28 (*sb*, 1H, amido –NH–); 7.72 (overlapped *d* and *s*, 2H, aroyl-*o*-phenyl); <sup>13</sup>C NMR (125 MHz, CDCl<sub>3</sub>) δ: 22.61; 22.84; 22.88; 22.96; 24.06; 24.63; 25.44; 25.54; 26.65;

29.35; 29.57; 32.12; 32.94; 33.16; 44.66; 47.50; 50.95; 65.45; 125.28; 129.08; 129.21; 134.82; 137.26; 142.78; 171.08; 199.07. ESI-MS HR: 397.2866 (M+1), Calc. 397.2849.

**4.2.34. *N*-cyclohexyl-4-oxo-2-(*R,S*)-1-imidazolyl-4-(5,6,7,8-tetrahydronaphthalenyl)butanamide (**34**)**

C<sub>23</sub>H<sub>29</sub>N<sub>3</sub>O<sub>2</sub>, starting from (*E*)-4-oxo-4-(5,6,7,8-tetrahydronaphthalenyl)-2-butenic acid cyclohexylamide (0.96 mmol) and a corresponding amount of imidazole, 0.210 g of **34** was obtained, 57.64% yield, as white solid, m.p. 98 °C (toluene). <sup>1</sup>H NMR (200 MHz, CDCl<sub>3</sub>) δ: 1.00–1.42 (*m*, 6H, 3,4-cyclohexyl –CH<sub>2</sub>–); 1.48–1.73 (*m*, 4H, 2-cyclohexyl –CH<sub>2</sub>–); 1.79 (*br*, 4H, tetralinoyl –CH<sub>2</sub>–); 2.78 (*br*, 4H, tetralinoyl –CH<sub>2</sub>–); 3.47 (*dd*, 1H, *J*<sub>1,2</sub> = 5.80, *J*<sub>1,3</sub> = 17.88, ABX); 3.61–3.83 (*m*, 1H, 1-cyclohexyl –CH–); 4.02 (*dd*, 1H, *J*<sub>1,2</sub> = 8.21, *J*<sub>1,3</sub> = 18.84, ABX); 5.42 (*t*, 1H, *J*<sub>1,2</sub> = 5.65, ABX); 6.80 (doublet-like signal, 1H, amido –NH–); 7.09 (*d*, 1H, *J* = 7.20, aroyl-*m*-phenyl); 7.14–7.29 (*m*, 3H, imidazolyl –CH–); 7.62 (*br*, 2H, aroyl-*m*-phenyl). <sup>13</sup>C NMR (50 MHz, CDCl<sub>3</sub>) δ: 22.58; 22.73; 24.60; 25.22; 29.17; 29.53; 32.47; 41.59; 48.74; 56.28; 95.70; 117.89; 125.05; 128.98; 129.40; 129.64; 133.39; 137.25; 137.57; 144.00; 167.42; 195.96. ESI-MS HR: 380.2337 (M+1), Calc. 380.2332.

**4.2.35. *N*-cyclohexyl-2-(*R,S*)-4-morpholinyl-4-oxo-4-(5,6,7,8-tetrahydro-2-naphthalenyl)butanamide (**35**)**

C<sub>24</sub>H<sub>34</sub>N<sub>2</sub>O<sub>3</sub>, starting from (*E*)-4-oxo-4-(5,6,7,8-tetrahydronaphthalenyl)-2-butan cyclohexylamide (0.96 mmol) and a corresponding amount of morpholine, 0.250 g of **35** was obtained, 65.12% yield, as white solid, m.p. 106–108 °C (toluene). <sup>1</sup>H NMR (500 MHz, CDCl<sub>3</sub>) δ: 1.14–1.24 (*m*, 3H, cyclohexyl –CH<sub>2</sub>–); 1.32–1.40 (*m*, 3H, cyclohexyl –CH<sub>2</sub>–); 1.58–1.62 (*m*, 1H, cyclohexyl –CH<sub>2</sub>–); 1.65–1.71 (*m*, 3H, cyclohexyl –CH<sub>2</sub>–); 1.81 (*m*, 4H, β-tetralinyl); 1.87 (*m*, 2H, cyclohexyl –CH<sub>2</sub>–); 2.58 (*m*, 4H, morpholinyl –CH<sub>2</sub>–); 2.80 (*m*, 4H, β-tetralinyl); 2.92 (*dd*, 1H, *J*<sub>1,2</sub> = 5.16, *J*<sub>1,3</sub> = 16.64, ABX); 3.63 (*dd*, 1H, *J*<sub>1,2</sub> = 7.08, *J*<sub>1,3</sub> = 16.45, ABX); 3.68 (*m*, 1H, cyclohexyl –CH–); 3.74 (*m*, 4H, morpholinyl –CH<sub>2</sub>–); 4.06 (*dd*, 1H, *J*<sub>1,2</sub> = 5.16, *J*<sub>1,3</sub> = 7.07, ABX); 7.23 (*m*, 1H, amido –NH–); 7.70–7.71 (overlapped *s* and *d*, 2H, aroyl-*o*-phenyl); <sup>13</sup>C NMR (125 MHz, CDCl<sub>3</sub>) δ: 22.83; 22.96; 24.69; 25.50; 29.37; 29.61; 32.52; 32.97; 33.26; 47.74; 50.07; 64.85; 67.35; 125.27; 128.20; 129.01; 129.09; 129.31; 134.59; 137.38; 143.11; 170.21; 198.46. ESI-MS HR: 399.2640 (M+1), Calc. 399.2648.

**4.2.36. *N*-cyclohexyl-2-(*R,S*)-[1-(4-methylpiperazinyl)]-4-oxo-4-(5,6,7,8-tetrahydronaphthalenyl)butanamide (**36**)**

C<sub>25</sub>H<sub>37</sub>N<sub>3</sub>O<sub>2</sub>, starting from (*E*)-4-oxo-4-(5,6,7,8-tetrahydronaphthalenyl)-2-butanic acid cyclohexylamide (0.96 mmol) and a corresponding amount of *N*-methylpiperazine, 0.130 g of **36** was obtained, 32.79% yield, as pale orange solid, m.p. 93–94 °C (toluene). <sup>1</sup>H NMR (500 MHz, CDCl<sub>3</sub>) δ: 1.18 (*m*, 2H, ax C2, cyclohexyl –CH–); 1.35 (*m*, 2H, ax C3, cyclohexyl –CH–); 1.37 (*m*, 1H, ax C4, cyclohexyl –CH–); 1.58 (*m*, 1H, eq C4, cyclohexyl –CH–); 1.67 (*m*, 2H, eq C3, cyclohexyl –CH–); 1.80 (doublet-like signal, 4H, β-tetralinyl); 1.86 (*m*, 2H, eq C2, cyclohexyl –CH–); 2.31 (*s*, 3H, piperazine-*N*-CH<sub>3</sub>); 2.50 (*br*, 4H, piperazine –CH<sub>2</sub>–); 2.61 (*br*, 4H, piperazine –CH<sub>2</sub>–); 2.80 (doublet-like signal, 4H, β-tetralinyl); 2.90 (*dd*, 1H, *J*<sub>1,2</sub> = 4.99, *J*<sub>1,3</sub> = 16.29, ABX); 3.60 (*dd*, 1H, *J*<sub>1,2</sub> = 7.59, *J*<sub>1,3</sub> = 16.69, ABX); 3.75 (*m*, 1H, cyclohexyl –CH–); 4.12 (*dd*, 1H, *J*<sub>1,2</sub> = 5.00, *J*<sub>1,3</sub> = 7.25, ABX); 7.09 (*d*, 1H, *J* = 8.67 Hz, amido –NH–); 7.12 (*d*, 1H, *J* = 9.20, aroyl-*m*-phenyl); 7.69 (*s*, 1H, aroyl-*o*-phenyl); 7.70 (*s*, 1H, aroyl-*o*-phenyl); <sup>13</sup>C NMR (125 MHz, CDCl<sub>3</sub>) δ: 22.83; 22.96; 24.67; 25.52; 29.35; 29.58; 32.15; 32.96; 33.23; 45.85; 47.64; 55.50; 125.24; 129.07; 129.23; 134.69; 137.28; 142.92; 170.43; 198.64. ESI-MS HR: 412.2951 (M+1), Calc. 412.2964.

#### 4.2.37. 2-(*R,S*)-(4-benzylpiperidinyl)-4-(4-isopropylphenyl)-4-oxo-*N*-phenylbutanamide (**37**)

C<sub>31</sub>H<sub>36</sub>N<sub>2</sub>O<sub>2</sub>, starting from (*E*)-4-(4-isopropylphenyl)-4-oxo-2-butenic acid phenylamide (0.7 mmol) and a corresponding amount of 4-benzylpiperidine, **37** was obtained, in quantitative yield, as a yellow semi-solid. <sup>1</sup>H NMR (500 MHz, CDCl<sub>3</sub>) δ: 1.26 (d, 6H, *J* = 7.06 Hz, *i*-PrCH<sub>3</sub>); 1.41 (*m*, 1H, piperidine –CH–); 1.72 (triplet-like, 4H, *J* = 13.63 Hz, piperidine –CH<sub>2</sub>–); 2.21 (*t*-like, 1H, *J* = 11.68 Hz, benzyl –CH<sub>2</sub>–); 2.45 (*t*-like, 1H, *J* = 11.19 Hz, benzyl –CH<sub>2</sub>–); 2.56 (*m*, 4H, piperidine –CH<sub>2</sub>–); 2.94 (overlapped *m*, 2H, ABX and *i*-PrCH); 3.68 (*dd*, 1H, *J*<sub>1,2</sub> = 6.81 Hz, *J*<sub>1,3</sub> = 16.30 Hz, ABX); 4.29 (*dd*, 1H, *J*<sub>1,2</sub> = 5.35 Hz, *J*<sub>1,3</sub> = 6.30 Hz, ABX); 7.08 (*t*, 1H, *J* = 7.50 Hz, benzyl-*p*-CH); 7.13 (*d*, 2H, *J* = 7.80 Hz, benzyl-*m*-phenyl); 7.19 (*t*, 1H, *J* = 6.37 Hz, amido-*p*-phenyl); 7.26 (*d*, 2H, *J* = 7.50 Hz, aroyl-*m*-phenyl); 7.29–7.32 (overlapped *m*, 4H, amido-*m*-phenyl and benzyl-*o*-phenyl); 7.53 (*d*, 2H, *J* = 7.50 Hz, amido-*o*-phenyl); 7.94 (*d*, 2H, *J* = 8.35 Hz, aroyl-*o*-phenyl); 9.39 (*s*, 1H, amido –NH–). <sup>13</sup>C NMR (125 MHz, CDCl<sub>3</sub>) δ: 21.42; 23.64; 30.68; 31.93; 32.85; 33.11; 34.21; 37.18; 37.57; 43.05; 45.12; 48.01; 52.75; 65.48; 119.29; 123.95; 125.91; 126.65; 128.21; 128.50; 128.94; 129.02; 134.90; 137.77; 140.24; 154.47; 170.47; 198.28. ESI-MS HR: 469.2852 (M+1), Calc. 469.2855.

#### 4.2.38. *N*-(3,5-dimethoxyphenyl)-2-(*R,S*)-[4-(2-dimethylaminoethyl)-1-piperazinyl]-4-(4-isopropylphenyl)-4-oxo-butanamide (**38**)

C<sub>29</sub>H<sub>42</sub>N<sub>4</sub>O<sub>4</sub>, starting from (*E*)-4-(4-isopropylphenyl)-4-oxo-2-butenic acid (3,5-dimethoxyphenyl)amide (0.57 mmol) and a corresponding amount of 4-(2-*N,N*-di-Me-aminoethyl)-1-piperazine, **38** was obtained, in quantitative yield, as a yellow semi-solid. <sup>1</sup>H NMR (500 MHz, CDCl<sub>3</sub>) δ: 1.27 (*d*, 6H, *J* = 7.33 Hz, *i*-PrCH<sub>3</sub>); 2.24 (*s*, 6H, *N*-(CH<sub>3</sub>)<sub>2</sub>); 2.43 (*m*, 2H, linker –CH<sub>2</sub>–); 2.48 (*m*, 2H, linker –CH<sub>2</sub>–); 2.59 (*br*, 4H, piperazine –CH<sub>2</sub>–); 2.67 (*br*, 4H, piperazine –CH<sub>2</sub>–); 2.97 (*m*, 1H, *J*<sub>1,2</sub> = 6.60 Hz, *J*<sub>1,3</sub> = 13.56 Hz, *i*-PrCH); 3.01 (*dd*, 1H, *J*<sub>1,2</sub> = 5.13 Hz, *J*<sub>1,3</sub> = 17.23 Hz, ABX); 3.68 (*dd*, 1H, *J*<sub>1,2</sub> = 6.96 Hz, *J*<sub>1,3</sub> = 17.23 Hz, ABX); 3.77 (*s*, 6H, –OCH<sub>3</sub>); 4.31 (*dd*, 1H, *J*<sub>1,2</sub> = 4.77 Hz, *J*<sub>1,3</sub> = 7.33 Hz, ABX); 6.22 (*t*, 1H, *J* = 2.19 Hz, amido-*p*-phenyl); 6.78 (*s*, 2H, amido-*o*-phenyl); 7.32 (*d*, 2H, *J* = 8.14, aroyl-*m*-phenyl); 7.94 (*d*, 2H, *J* = 8.46, aroyl-*o*-phenyl); 9.29 (*s*, 1H, amido –NH–). <sup>13</sup>C NMR (125 MHz, CDCl<sub>3</sub>) δ: 23.60; 31.85; 45.61; 54.16; 55.36; 56.47; 56.82; 64.55; 96.36; 97.49; 126.64; 128.15; 128.45; 128.96; 134.73; 139.48; 154.59; 161.04; 170.06; 197.72. ESI-MS HR: 511.3283 (M+1), Calc. 511.3284.

#### 4.3. Anticholinesterase activity assay

The inhibition potency of the compounds **1–38** toward AChE was evaluated by Ellman procedure [28], using the enzyme from electric eel, type VI-S (Sigma) and acetylthiocholine iodide (0.28 mM) as substrate. Four to six different concentrations, which produce 20–80% of enzyme activity inhibition, of the each compound were used. The reaction took place in the final volume of 2 mL of 0.1 M potassium phosphate buffer, pH 8.0, containing 0.03 units of AChE and 0.3 mM 5,5'-dithiobis(2-nitrobenzoic)acid (DTNB), used to produce yellow anion of 5-thio-2-nitrobenzoic acid in reaction with thiocholine released by AChE. Test compound was added to the enzyme solution and preincubated at 25 °C for 35 min, followed by the addition of DTNB (0.95 mL) and substrate (50 μL). Inhibition curves were performed at least in triplicate. One triplicate sample without test compound was always present to yield 100% of AChE activity. The reaction was monitored for 3 min, and the color production was measured at 412 nm. The reaction rates were compared, and the percent of inhibition, due to the presence of test compounds, was calculated. IC<sub>50</sub> values were determined

from inhibition curves (log inhibitor concentration vs. percent inhibition).

The investigation of butyrylcholinesterase inhibition was carried out similarly, using 0.035 units of horse serum BChE (Sigma) and 0.5 mM butyrylthiocholine iodide, in final volume of 2 mL.

For determination of inhibition type for compound **17**, the Lineweaver–Burk plots were generated by using a fixed amount of acetylcholinesterase and varying amounts of the substrate (0.10–0.20 mM), in the absence or presence of different inhibitor concentrations. The re-plots of the slopes and intercepts of the double reciprocal plots against inhibitor concentrations gave the inhibitor constants (*K*<sub>i1</sub> and *K*<sub>i2</sub>, for the binding to free enzyme and enzyme substrate complex) as the intercepts on the *x*-axis.

#### 4.4. Molecular modeling

The 3D-QSAR model for the set of the selected compounds was built using Pentacle program. Protonation state of the each compound was ascribed by the program under pH 8.00, the same as used in biological assay. Pentacle uses AMANDA [29] algorithm to produce the second generation of alignment-independent molecular descriptors (GRIND-2). Descriptors are obtained from GRID [30] molecular interaction fields (MIF's). Derived GRID MIF minima are encoded in the descriptors. Descriptors consist of pair of nodes, including interaction energy (IE) of each node and the distance between nodes. Descriptors are further processed by means of built-in PCA/PLS (principal component/partial least squares) statistical tool. For model generation all available (DRY, O, N1 and TIP) probes were used, with GRID resolution of 0.5 Å. For the encoding, CLAC algorithm was applied. Predictivity of the model was assessed by using leave-one-out, leave-two-out or cross-validation using four groups of compounds of the approximately same size, in which the objects were assigned randomly.

Docking is a procedure for predicting the interaction and the mode of ligand binding to biomacromolecular targets. AutoDock 4.2 uses a semi-empirical free energy force field to evaluate conformations during docking calculations. The program requires pre-calculated grid maps, one for each atom type present in the ligand being docked. This helps to make the docking calculations fast. These maps are calculated by AutoGrid. A grid map consists of a three-dimensional lattice of regularly spaced points, surrounding (either entirely or partly) and centered on some region of interest of the macromolecule under study. AutoDock uses one of several conformational search algorithms to explore the conformational states of a flexible ligand, using the maps generated by AutoGrid to evaluate the ligand–protein interaction at each point in the docking simulation. In a typical docking, the user will dock a ligand several times, to obtain multiple docked conformations. The results may be clustered to identify similar conformations. Docking experiments for compounds **6**, **17** and **18** were performed on the *M. musculus* AChE structure, refined at 2.05 Å resolution (PDB entry 2HA2). Truncated residues were properly completed by means of Swiss PDB Viewer [31]. Hydrogen atoms were added to the protein amino acid residues, non-polar hydrogens were merged, and Gas-teiger charges were ascribed using AutoDock Tools [32]. The lowest energy conformations of the compounds were generated using OMEGA software [33]. Both enantiomers of the each compound were docked into mAChE active site gorge, using AutoDock 4.0.1 package [25]. Docking was carried out by using hybrid Lamarckian genetic algorithm; 50 runs were performed with an initial population of 250 randomly placed individuals and maximum number of 2.5 × 10<sup>6</sup> energy evaluations. Resulting docked poses within RMSD of 0.5 Å were clustered together. All other parameters were maintained at their default settings. The docking calculations were also performed using Glide extra precision (XP) protocol



(Schrödinger) [34,35]. Due to the fact that this procedure provided docking poses very similar to poses obtained by AutoDock, these results are not shown. Docking of compounds **16** and **20** were done following the same computational set-up as described for AChE, using HuBChE crystal structure (PDB entry 1POI).

For the molecular dynamics simulations, the most populated docking pose of the (S)-enantiomer of compound **18**, retrieved by AutoDock, was used. The system was neutralized in VegaZZ [36] by addition of explicit sodium counterions, and afterward embedded in a cluster that surrounds the protein with a layer of 75 Å water molecules. For molecular dynamics simulations, NAMD 2.9 [37] was used, with CHARMM22 force field and Gasteiger's atomic charges. The system was minimized in 30,000 steps (30 ps) by conjugate gradient algorithm and, afterwards, heated to 300 K during 10,000 steps (10 ps). The 10 ns of unconstrained, productive, molecular dynamics simulations was performed, at  $300 \pm 10$  K (Langevin's algorithm), using periodic boundary conditions. Electrostatics was treated by a Particle Mesh Ewald algorithm. Cut-offs were set to 12 Å for vdW interactions, with a switch starting at 8 Å, and pair list distance set to 13.5 Å. Trajectory frames were collected each ps to yield 10,000 frames per trajectory. All simulations were performed on the multi-node Linux based cluster [38] equipped with the dual Intel Xeon X5560 @ 2.8 GHz processors. Results were analyzed in VegaZZ as GUI, in Windows environment.

## Acknowledgments

This work was supported by the Ministry of Education, Science and Technological Development of the Republic of Serbia, grant No 172035. The computational work reported makes use of results produced by the High-Performance Computing Infrastructure for South East Europe's Research Communities (HP-SEE), a project co-funded by the European Commission (under Contract Number 261499) through the Seventh Framework Programme HP-SEE (<http://www.hp-see.eu/>). Authors gratefully acknowledge OpenEye Scientific Software, Santa Fe, NM, for the free academic licensing of software tools. Authors gratefully acknowledge computational time provided on HPCG cluster located at Institute of Information and Communication Technologies of the Bulgarian Academy of Science (IICT-BAS), and Prof. Thomas Mavromoustakos (Department of Chemistry, University of Athens) for kindly providing us the Glide program.

## Appendix A. Supplementary data

Supplementary data related to this article can be found online at <http://dx.doi.org/10.1016/j.ejmech.2014.05.008>.

## References

- [1] A.V. Terry Jr., J.J. Buccafusco, The cholinergic hypothesis of age and Alzheimer's disease - related cognitive deficits: recent challenges and their implications for novel drug development, *J. Pharm. Exp. Ther.* 306 (2003) 821–827.
- [2] A.R. Punga, E. Stalberg, Acetylcholinesterase inhibitors in myasthenia gravis: to be or not to be? *Muscle Nerve* 39 (2009) 724–728.
- [3] L.A. Sorbera, J. Aravamundan, C. Dulsat, *Drug. Future* 35 (2010) 585–595.
- [4] G.A. Petroianu, K. Arafat, A. Schmitt, M.Y. Hassan, Weak inhibitors protect cholinesterases from strong inhibitors (paraoxon): in vitro effect of ranitidine, *J. Appl. Toxicol.* 25 (2005) 60–67.
- [5] Y. Meshulam, G. Cohen, S. Chapman, D. Alhalai, A. Levy, Prophylaxis against organophosphate poisoning by sustained release of scopolamine and physostigmine, *J. Appl. Toxicol.* 21 (2001) S75–S78.
- [6] M.M. Mesulam, A. Guillozet, P. Show, A. Lavey, E.G.M. Duysen, O. Lockridge, Acetylcholinesterase knockouts establish central cholinergic pathways and can use butyrylcholinesterase to hydrolyze acetylcholine, *Neuroscience* 110 (2002) 627–639.
- [7] B. Li, J.A. Stribley, A. Ticu, W. Xie, L.M. Shopfer, P. Hammond, S. Brimjoin, S.H. Henrichs, O. Lockridge, Abundant tissue butyrylcholinesterase and its possible function in the acetylcholinesterase knockout mouse, *J. Neurochem.* 75 (2000) 1320–1331.
- [8] S.S. Jhee, T. Shiofritz, R.D. Hartman, J. Mesina, R. Anand, J. Sramek, N.R. Cutler, Centrally acting antiemetics mitigate nausea and vomiting in patients with Alzheimer's disease who receive rivastigmine, *Clin. Neuropharmacol.* 25 (2002) 122–123.
- [9] E.K. Perry, R.H. Perry, G. Blessed, B.E. Tomlinson, Changes in brain cholinesterases in senile dementia of Alzheimer type, *Neuropathol. Appl. Neurobiol.* 4 (1978) 273–277.
- [10] G. Gibney, S. Camp, M. Dionne, K. MacPhee-Quigley, P. Taylor, Mutagenesis of essential functional residues in acetylcholinesterase, *Proc. Natl. Acad. Sci. U. S. A.* 87 (1990) 7546–7550.
- [11] M. Ekholm, H. Konsch, Comparative model building of human butyrylcholinesterase, *J. Mol. Struct. Teochem* 467 (1990) 161–172.
- [12] A. Ordentlich, D. Barak, C. Kronman, N. Ariel, Y. Segall, B. Velan, A. Shafferman, Functional characteristics of the oxyanion hole in human acetylcholinesterase, *J. Biol. Chem.* 273 (1998) 19509–19517.
- [13] H.J. Kreienkamp, C. Weise, R. Raba, A. Aaviksaar, F. Hucko, Anionic subsites of the catalytic center of acetylcholinesterase from Torpedo and from cobra venom, *Proc. Natl. Acad. Sci. U. S. A.* 88 (1991) 6117–6121.
- [14] C. Weise, H.J. Kreienkamp, R. Raba, A. Pedak, A. Aaviksaar, F. Hucko, Anionic subsites of the acetylcholinesterase from Torpedo californica: affinity labeling with cationic reagent *N,N*-dimethyl-2-phenyl-aziridinium, *EMBO J.* 9 (1990) 3885–3888.
- [15] J.L. Sussman, M. Harel, F. Frolow, C. Oefner, A. Goldman, L. Toker, I. Silman, Atomic structure of acetylcholinesterase from Torpedo californica: a prototypic acetylcholine-binding protein, *Science* 253 (1991) 872–879.
- [16] A. Ordentlich, D. Barak, C. Kronman, U. Flashner, M. Leitner, Y. Segall, N. Ariel, S. Cohen, B. Velan, A. Shafferman, Dissection of the human acetylcholinesterase active center determinants of substrate specificity. Identification of residues constituting the anionic site, the hydrophobic site and the acyl pocket, *J. Biol. Chem.* 268 (1993) 17083–17095.
- [17] D.C. Velom, Z. Radić, L. Ying, N.A. Pickering, S. Camp, P. Taylor, Aminoacid residues controlling acetylcholinesterase and butyrylcholinesterase specificity, *Biochemistry* 32 (1993) 12–17.
- [18] P. Taylor, S. Lappi, Interaction of fluorescence probes with acetylcholinesterase. Site and specificity of propidium binding, *Biochemistry* 14 (1975) 1989–1997.
- [19] D. Barak, C. Kronman, A. Ordentlich, A. Naomi, A. Bromberg, D. Marcus, A. Lazar, B. Velan, A. Shafferman, Acetylcholinesterase peripheral anionic site degeneracy conferred by amino acid arrays shearing a common core, *J. Biol. Chem.* 269 (1994) 6296–6305.
- [20] Y. Bourne, P. Taylor, Z. Radić, P. Marchot, Structural insights into ligand interactions at the acetylcholinesterase peripheral anionic site, *EMBO J.* 22 (2003) 1–12.
- [21] A. Saxena, A.M.G. Redman, X. Jiang, O. Lockridge, B.P. Doctor, Differences in active site gorge dimensions of cholinesterase revealed by binding of inhibitors to human butyrylcholinesterase, *Biochemistry* 36 (1997) 14642–14651.
- [22] M.D. Vitorović-Todorović, I.O. Juranić, Lj. M. Mandić, B.J. Drakulić, 4-Aryl-4-oxo-N-phenyl-2-aminylbutyramides as acetyl- and butyrylcholinesterase inhibitors. Preparation, anticholinesterase activity, docking study, and 3D structure-activity relationship based on molecular interaction fields, *Bioorg. Med. Chem.* 18 (2010) 1181–1193.
- [23] D. Papa, E. Schwenk, F. Villani, E. Klingsberg,  $\beta$ -Aroylacrylic acids, *J. Am. Chem. Soc.* 70 (1948) 3356–3360.
- [24] P. Kulsa, D.R. Hoff, H.H. Mrozik, U. S. Pat. 4, 130, 661, Merck & Co., Inc. Rahway, N.J., 1977.
- [25] G.M. Morris, R. Huey, W. Lindstrom, M.F. Sanner, R.K. Belew, D.S. Goodsell, A.J. Olson, Autodock4 and AutoDockTools4: automated docking with selective receptor flexibility, *J. Comp. Chem.* 16 (2009) 2785–2791.
- [26] (a) G.L. Warren, C.W. Andrews, A.-M. Capelli, B. Clarke, J. LaLonde, M.H. Lambert, M. Lindvall, N. Nevins, S.F. Semus, S. Senger, G. Tedesco, I.D. Wall, J.M. Woolven, C.E. Peishoff, M.S. Head, A critical assessment of docking programs and scoring functions, *J. Med. Chem.* 49 (2006) 5912–5931; (b) G. Schneider, Virtual screening: an endless staircase? *Nat. Rev. Drug Discov.* 9 (2010) 273–276.
- [27] A.C. Wallace, R.A. Laskowski, J.M. Thornton, LIGPLOT: a program to generate schematic diagrams of protein-ligand interactions, *Prot. Eng.* 8 (1995) 127–134.
- [28] L.G. Ellman, K.D. Courtney, V. Andres Jr., M.R. Featherstone, A new and rapid colorimetric determination of acetylcholinesterase activity, *Biochem. Pharm.* 2 (1961) 88–95.
- [29] A. Duran, G.C. Martinez, M. Pastor, Development and validation of AMANDA, a new algorithm for selecting highly relevant regions in molecular interaction fields, *J. Chem. Inf. Model.* 48 (2008) 1813–1823. Pentacle 1.0.6, [www.moldiscovery.com](http://www.moldiscovery.com).
- [30] P.J. Goodford, A computational procedure for determining energetically favorable binding sites on biologically important macromolecules, *J. Med. Chem.* 28 (1985) 849–857. GRID 2.2c, <http://www.moldiscovery.com>.
- [31] N. Guex, M.C. Peitsch, SWISS-MODEL and the Swiss-PdbViewer: an environment for comparative protein modeling, *Electrophoresis* 18 (1997) 2714–2723. <http://www.expasy.org/spdv>.
- [32] M.F. Sanner, Python: a programming language for software integration and development, *J. Mol. Graph. Model.* 17 (1999) 57–61.

- [33] a) P.C.D. Hawkins, A.G. Skillman, G.L. Warren, B.A. Ellingson, M.T. Stahl, Conformer generation with OMEGA: algorithm and validation using high quality structures from the protein databank and Cambridge structural database, *J. Chem. Inf. Model.* 50 (2010) 572–584;  
b) P.C.D. Hawkins, A. Nicholls, Conformer generation with OMEGA: learning from the data set and the analysis of failures, *J. Chem. Inf. Model.* 52 (2012) 2919–2936. OMEGA v. 2.4.2, OpenEye Scientific Software, Santa Fe, NM, <http://www.eyesopen.com>.
- [34] R.A. Friesner, R.B. Murphy, M.P. Repasky, L.L. Frye, J.R. Greenwood, T.A. Halgren, P.C. Sanschagrin, D.T. Mainz, Extra precision Glide: docking and scoring incorporating a model of hydrophobic enclosure for protein-ligand complexes, *J. Med. Chem.* 49 (2006) 6177–6196.
- [35] Glide, Small-Molecule Drug Discovery Suite, Schrödinger, LLC, New York, NY., 2012.
- [36] A. Pedretti, L. Villa, G. Vistoli, Vega – an open platform to develop chemo-bio-informatics applications, using plug-in architecture and script programming, *J. Comput. Aided Mol. Des.* 18 (2004) 167–173. <http://www.ddl.unimi.it>.
- [37] J.C. Phillips, R. Braun, W. Wang, J. Gumbart, E. Tajkhorshid, E. Villa, C. Chipot, R.D. Skeel, L. Kalé, K. Schulten, Scalable molecular dynamics with NAMD, *J. Comput. Chem.* 26 (2005) 1781–1802. <http://www.ks.uiuc.edu/Research/namd/>.
- [38] E. Atanassov, T. Gurov, A. Karaivanova, Capabilities of the HPC cluster at IICT-BAS, *Automatika Informatika* 2 (2011) 7–11 (in Bulgarian).